Hindawi
Journal of Sensors
Volume 2021, Article ID 6640077, 24 pages
https://doi.org/10.1155/2021/6640077

Research Article

Integration of Multiband InSAR and Leveling Measurements for Analyzing the Surface Subsidence of Shield Tunneling at Beijing-Zhangzhou High-Speed Railway

Yueguan Yan[1], **Qian Yang**[1], **Zhihui Jia**[1,2], **Xiaoyi Zhang**[3], **Huayang Dai**[1] and **Alex Hay-Man Ng**[4,5]

[1]*College of Geoscience and Surveying Engineering, China University of Mining & Technology (Beijing), Beijing 100083, China*
[2]*Beijing Vastitude Technology Co., Ltd., 100191, Beijing 100191, China*
[3]*Beijing Tiejian Project Management Ltd., 100036, Beijing 100055, China*
[4]*School of Civil and Transportation Engineering, Guangdong University of Technology, Guangzhou 510006, China*
[5]*Key Laboratory for City Cluster Environmental Safety and Green Development of the Ministry of Education, Institute of Environmental and Ecological Engineering, Guangdong University of Technology, Guangzhou 510006, China*

Correspondence should be addressed to Alex Hay-Man Ng; hayman.ng@gdut.edu.cn

Received 22 November 2020; Revised 29 March 2021; Accepted 7 April 2021; Published 28 June 2021

Academic Editor: Jesús Lozano

In modern life, metro and high-speed rails have become indispensable transportation and have been playing an important role in many areas, especially in cities. The metro and high-speed rails have varying degrees of impact on the surface and surrounding buildings, which must be carefully understood to minimize the risk of hazards. This work is aimed at investigating the deformation of ground surface and the surrounding structures, caused by the excavation of underground tunnels. Because of the spatiotemporal characteristics of the land subsidence induced by underground tunnel construction, the measurements obtained from InSAR (Synthetic Aperture Radar Interferometry) and leveling techniques are integrated to study the subsidence phenomenon of the ground surface above the shield tunnels and the surrounding buildings. The subsidence-related parameters, including the advance angles, lag angles, and boundary angles, are derived from the deformation results. This study suggests that leveling and InSAR observations can provide technical support to study the subsidence of dense buildings on the surface of shield tunnel excavation and to protect the surrounding environment.

1. Introduction

Land subsidence is the loss of elevation caused by natural and human factors. The land subsidence issue, especially in urban areas, has a great impact on the environment and resources as well as human life. Urban development and expansion, caused by the rapid population growth, often adds pressure to the existing transportation system. Many cities (e.g., Beijing, Shanghai, Guangzhou, and Tokyo) in the world increasingly rely on the underground transportation systems in order to reduce the issues due to traffic congestion, noise and air pollution, and densely built-up urban areas. Amongst all urban underground tunnel construction techniques, shield tunneling technology has been widely used because of its fast, convenient, efficient, and small impact [1]. However, such a construction technique can affect the stability of the ground surface and buildings near the construction area. Therefore, it is necessary to monitor the ground surface and buildings near the shield tunnel construction area and understand their subsidence characteristics, for example, observing the subsidence of the ground near the shield tunnel.

Leveling is the most common technique used for subsidence monitoring of the ground surface and buildings above

the shield tunnels, which has been successfully demonstrated in many applications [2–6]. Conventional surveying techniques such as leveling can provide the reliable measurement data precisely, but they are not suitable for monitoring the ground subsidence which reminds us to measure long term and broadly because of its inefficient observation and massive work.

InSAR is a remote sensing technique that has been widely recognized because of its capability for monitoring ground deformation under all-weather conditions, with wide coverage and high precision [7, 8]. Time-series InSAR (TS-InSAR), an extension of the InSAR technique, can be used to obtain the deformation time series of ground features such as transportation infrastructures. It has been widely used to monitor land subsidence caused by various reasons [9–17]. Many of these studies suggest that the precision of the subsidence monitoring results can be affected by poor working conditions. Many researchers have suggested different approaches to deal with this issue, for example, utilization of multiband InSAR data [18] and integrating multiple subsidence monitoring methods [19, 20].

Through the reading and analysis of existing articles, it is found that there are very few studies that utilize both leveling and InSAR (multiband SAR data) to study and analyze the deformation of the ground caused by shield tunnel excavation and the impact of buildings (structures) near the tunnel. Since the two techniques have different strengths (spatial and temporal coverage for InSAR and accuracy for leveling) and weaknesses (various biases for InSAR, notably atmospheric, while very limited spatial and temporal coverage for leveling), therefore, using a single deformation monitoring technique is often not enough to deliver the comprehensive ground subsidence phenomenon caused by underground tunnel excavation. Combining multiple ground subsidence measurements is one possible solution to this issue.

In order to obtain the comprehensive knowledge of the ground subsidence phenomenon due to underground construction, it is important to obtain the parameters related to underground construction-induced subsidence (Table 1). The objective of this work is to develop a framework to derive the subsidence-related parameters by integrating the leveling and InSAR techniques and apply them to investigate the ground subsidence at the Beijing-Zhangzhou high-speed railway shield tunnel. The shield tunnel in the study area is close to the existing subway lines in Beijing that is surrounded by dense buildings. Therefore, it is of great interest to study the deformation of ground surface and infrastructure caused by the excavation of shield tunnels and to investigate the impact of shield tunnel excavation on the surrounding environment caused by ground subsidence.

This manuscript is arranged as follows. First, the subsidence-related parameters, useful to study the characteristics of subsidence phenomenon of the ground surface above the shield tunnels and the surrounding buildings, are investigated. Since different subsidence monitoring techniques, such as leveling and InSAR, have their own strengths and weaknesses, the suitability of these techniques for obtaining each parameter is assessed based on the features of the subsidence phenomenon caused by underground construction. Next, a case study is conducted based on this framework to monitor the ground surface and surrounding buildings and infrastructures above the shield tunnels. Then, the temporal change characteristics of the structures on the upper surface of the shield tunnel and the surrounding area are obtained, and the subsidence law of the shield tunnel excavation is understood. This information is expected to be important for providing technical support for shield tunnel excavation and security for safe construction.

2. Methods

2.1. The Characteristics of Land Surface Caused by Shield Tunnel Excavation and Their Subsidence-Related Parameters. For the land subsidence caused by shield excavation, the maximum ground surface subsidence generally occurs in the center of the tunnel on the cross-section of its advancing direction. The amount of subsidence gradually decreases as it gets further away from the center of the tunnel. For the case of the longitudinal section of its advancing direction, the initial subsidence is often small, and then the surface subsidence begins to accelerate. Then, the rate of ground subsidence decreases until the rate becomes zero. Finally, after the surface subsidence reaches the maximum, the subsidence tends to stabilize.

Subsidence-related parameters are very important in analyzing the impacts and subsidence phenomenon due to underground construction, and the reliability of subsidence forecasts and risk assessments. The definition of the subsidence-related parameters, the methods of obtaining these parameters, and the role of the parameters are shown in Table 1.

2.2. The Characteristics of Leveling and InSAR Technology. Leveling is the one of the most popular monitoring methods for surface deformation, and it can achieve high precision and high frequency observation of surface subsidence in a small area. However, there are several limitations of leveling when comparing to InSAR. Mainly, they are reflected in the following aspects:

(1) Deformation monitoring is difficult to implement and is often restricted by terrain and weather conditions

(2) It is difficult to monitor a large area in a short time, and it is easy to cause accumulated errors

(3) It is only capable for discrete point monitoring, so it can only obtain the deformation information of the monitoring points. The deformation information of the unmonitored points needs to be obtained by a difference method

In this study, the surface subsidence of the Beijing-Zhangzhou high-speed railway shield tunnel is studied using the leveling data. The total length of the railway shield tunnel is about 4 km. There are 45 cross-sections with more than 5 measuring points. The monitoring ranges of the cross-sectional sections are 6-11 m on both sides of the tunnel. The layout of leveling points in the cross-section direction is shown in Figure 1. The black triangles are the leveling points.

Table 1: The feasibility of the leveling and InSAR methods for deriving the various subsidence-related parameters [21–23].

Subsidence-related parameters	Description	Measurement requirement	Suitable monitoring techniques	Effect
Angle of advance influence in longitudinal section	When the gob has reached the critical size, or nearly so, on the major cross-section of a movement basin, the critical line at the faceline and the line connecting the movement initiation point on the surface with the faceline is the angle of advance influence	High precision Frequent monitoring and real-time monitoring	Leveling	Determine the influence range of ground subsidence when the working face advances to any position in the process of advancing on the working surface
Lag distance of maximum subsidence rate	The distance between the maximum subsidence velocity point and the position of the working surface	High precision Real-time monitoring	Leveling	The point where the surface has the highest subsidence velocity is the place where the surface moves most violently at that time. Knowing the law of the lag angle, we can determine the area with the most violent ground movement at any time during the advancement of the working face
Lag angle of maximum subsidence rate	The angle between the line connecting the point with maximum subsidence velocity and the working face	High precision Real-time monitoring	Leveling	
Boundary of subsidence in transverse direction	The contour line of 2 mm of subsidence is used to define the edge of the surface movement	Medium precision Large area	Leveling and InSAR (C-band)	It is of great significance for controlling ground subsidence and protecting buildings by monitoring the ground surface and the sinking of ground building
Far field displacement	The far field displacement from the shield tunnel is usually small with long settlement time. This type of subsidence is usually far away from the tunnel	High precision Large area	InSAR (X-band)	
Subsidence duration, etc.	The time it takes for the ground surface to become stable at the maximum subsidence point	Relatively short monitoring time (6 days) Real-time monitoring Small area	Leveling	Determining the time range of drastic changes in the surface of the shield tunnel is of practical significance for the protection of the upper surface of the shield tunnel and the building

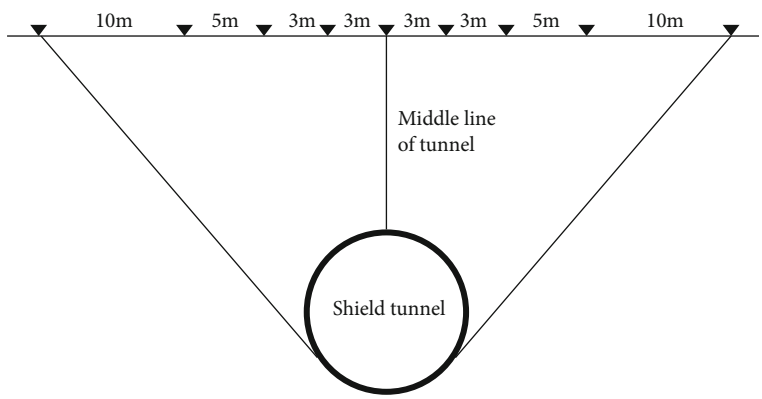

Figure 1: Cross-sectional directional leveling point layout.

InSAR technology has the characteristics of all-time, all-weather, high resolution, and regional spatial coverage. The TS-InSAR technology used in this work is an extension of InSAR technology. It has several advantages over leveling in land subsidence monitoring which includes the following:

(1) Low observation cost, since it does not require to invest a lot of manpower, materials, and financial resources to observe the subsidence and maintain the settlement monitoring points

(2) Relatively high spatial resolution (generally 10 m to 30 m) compared to conventional geodetic techniques

(3) Wide monitoring range—a single SAR image can cover hundreds of square kilometers

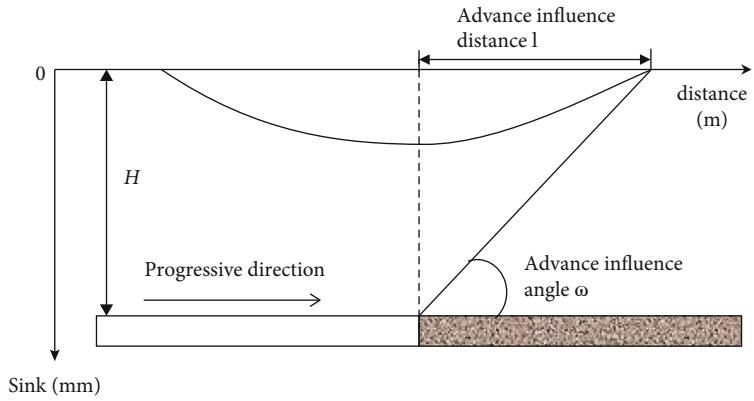

Figure 2: Advance influence angle and distance.

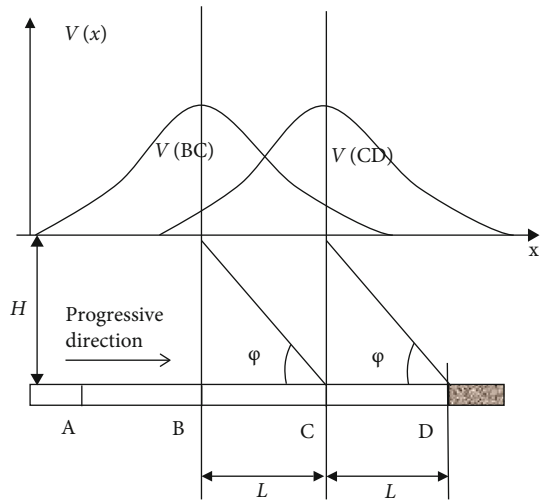

Figure 3: Subsidence curve and hysteresis effect during the advancing process of the working face.

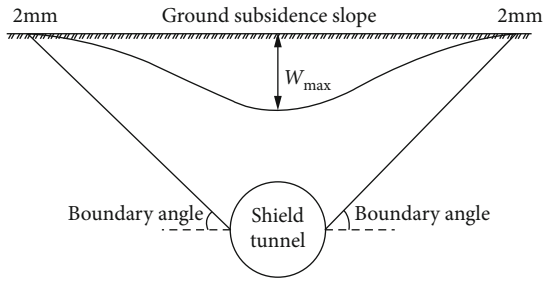

Figure 4: Boundary of subsidence in transverse direction.

(4) Monitoring continuity and periodic or nonperiodic long-term monitoring of the same target on the ground can be performed at a certain time interval to obtain the dynamic deformation process of the target in the time series. In addition, it is not affected by time and weather conditions and is possible to conduct measurement at all times

(5) High security, no need to establish ground monitoring points, and no need to touch the monitoring target; it can also monitor when server ground movement occurs

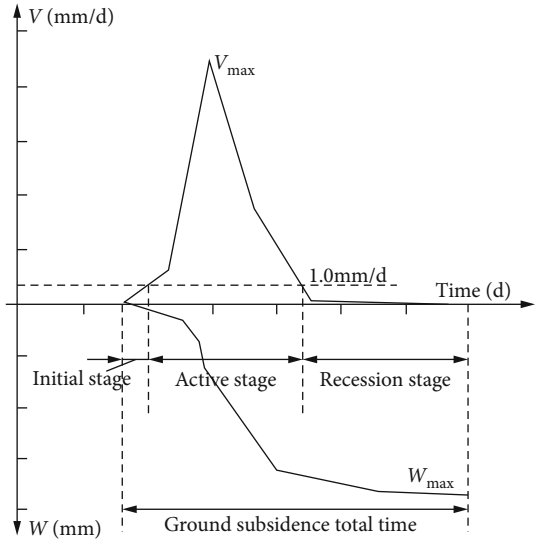

Figure 5: Surface subsidence time and velocity.

In short, InSAR can possibly meet some of the requirements for monitoring surface subsidence caused by shield tunnel exaction; therefore, it can be a useful supplement to the existing land subsidence monitoring technology.

2.3. Joint Methods to Derive the Subsidence-Related Parameters. In order to study the subsidence phenomenon of the ground surface above the underground activities, it is important to derive the subsidence-related parameters, e.g., advance influence angle, lag distance, and angle of maximum subsidence rate, that are often used to describe the subsidence characteristics of the shield tunnel excavation. In this work, a framework is proposed to integrate leveling and InSAR monitoring in order to derive these subsidence-related parameters. The basic concept is to derive different subsidence-related parameters using different monitoring methods (i.e., leveling and InSAR). The monitoring methods can be selected according to their strengths and shortcomings as

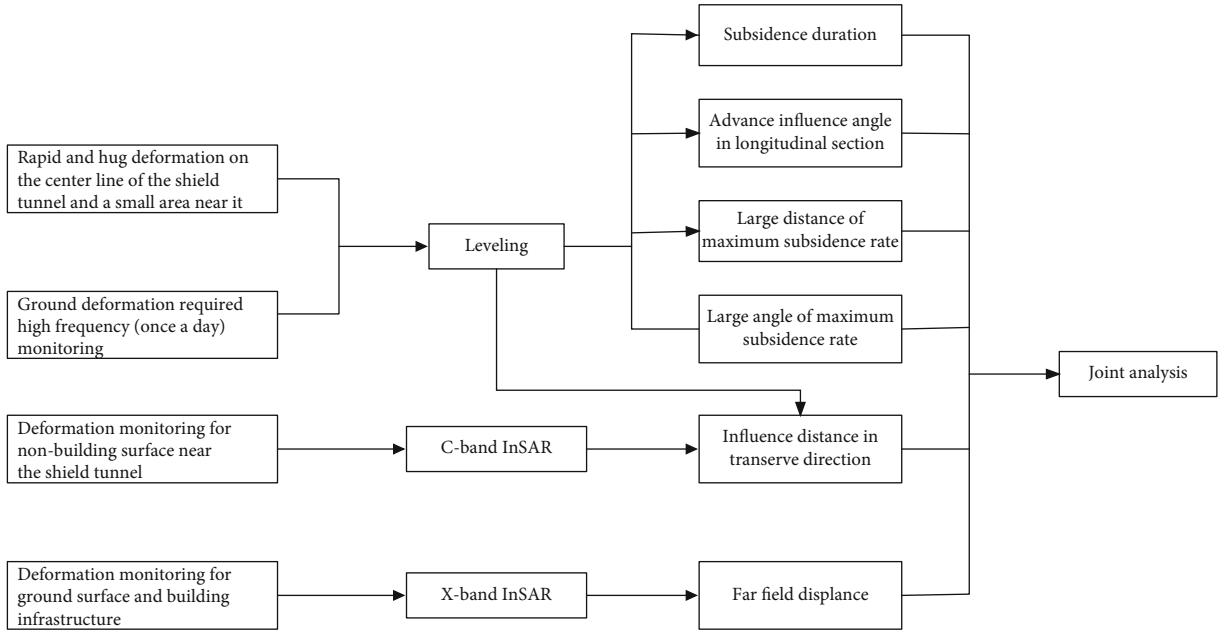

Figure 6: The method of joint analysis.

well as the measurement requirements. The parameters of land subsidence are as follows.

2.3.1. Advance Influence Angle and Distance. Advance influence angle is one of the subsidence-related parameters. It is possible to understand the meaning of this parameter through the following figure: In the process of working face recommendation, the ground surface in front of the working face sinks under the influence of mining. This phenomenon is called advanced influence. The line between the point where the ground surface starts to move (the value of subsidence is 10 mm) in front of the working face and the current working face. The angle between this line and the horizontal line on the side of the tunnel excavation direction is called the advanced influence angle, expressed by ω. The horizontal distance from the starting point to the working surface is called advance influence distance, expressed by the advance influence distance. We can understand the advance influence angle and distance with the help of Figure 2. In Figure 2, the direction of the arrow is the advancing direction of the shield tunnel; the white rectangle at the bottom of Figure 2 represents the shield tunnel that has been excavated, and the gray rectangle is the unexcavated section.

2.3.2. Lag Distance and Lag Angle of Maximum Subsidence Rate. In the surface movement of coal mining, the hysteresis of the maximum subsidence speed refers to the phenomenon that the position of the maximum surface subsidence rate point is always behind the working surface by a certain distance on the surface subsidence rate curve. This distance is called the lag distance of maximum subsidence rate. The lag angle of the maximum subsidence rate refers to the angle between the line between the working face and the maximum land subsidence rate point and the side of the coal seam goaf, denoted by φ. According to the definition of the lag distance and the lag angle of the maximum subsidence rate in the process of coal mining, the lag distance and the angle of maximum subsidence rate in the shield tunnel excavation process are defined, as shown in Figure 3. In Figure 3, the direction of the arrow is the advancing direction of the shield tunnel, the white rectangle at the bottom of the Figure 3 represents the shield tunnel that has been excavated, and the gray rectangle is the unexcavated section.

2.3.3. Boundary of Subsidence in Transverse Direction. Theoretically, the moving basin boundary is defined as the basin boundary point with 0 surface movement and deformation. However, in general, the boundary surrounded by the sinking point of 10 mm is regarded as the boundary of the moving basin.

On the cross-section in the forward direction of shield tunnel excavation, the boundary point of the influence range is the point at which the ground subsidence value is 2 mm (Figure 4).

2.3.4. Subsidence Duration. The surface subsidence time is the time it takes for the land movement at the maximum subsidence point to stabilize from the beginning of the movement process. The whole movement process at a ground surface point can be divided into three stages based on the change of the surface subsidence rate (as shown in Figure 5): (1) the initial stage (ground subsidence rate from stabilization to 1 mm/day), (2) the active stage (subsidence rate from 1 mm/day to the maximum subsidence rate and then to 1 mm/day), and (3) the recession stage (subsidence rate from 1 mm/day to stabilization). Surface subsidence time is the total time of these three stages.

2.4. The Framework of Joint Monitoring Methods. As mentioned above, InSAR technology with leveling technology

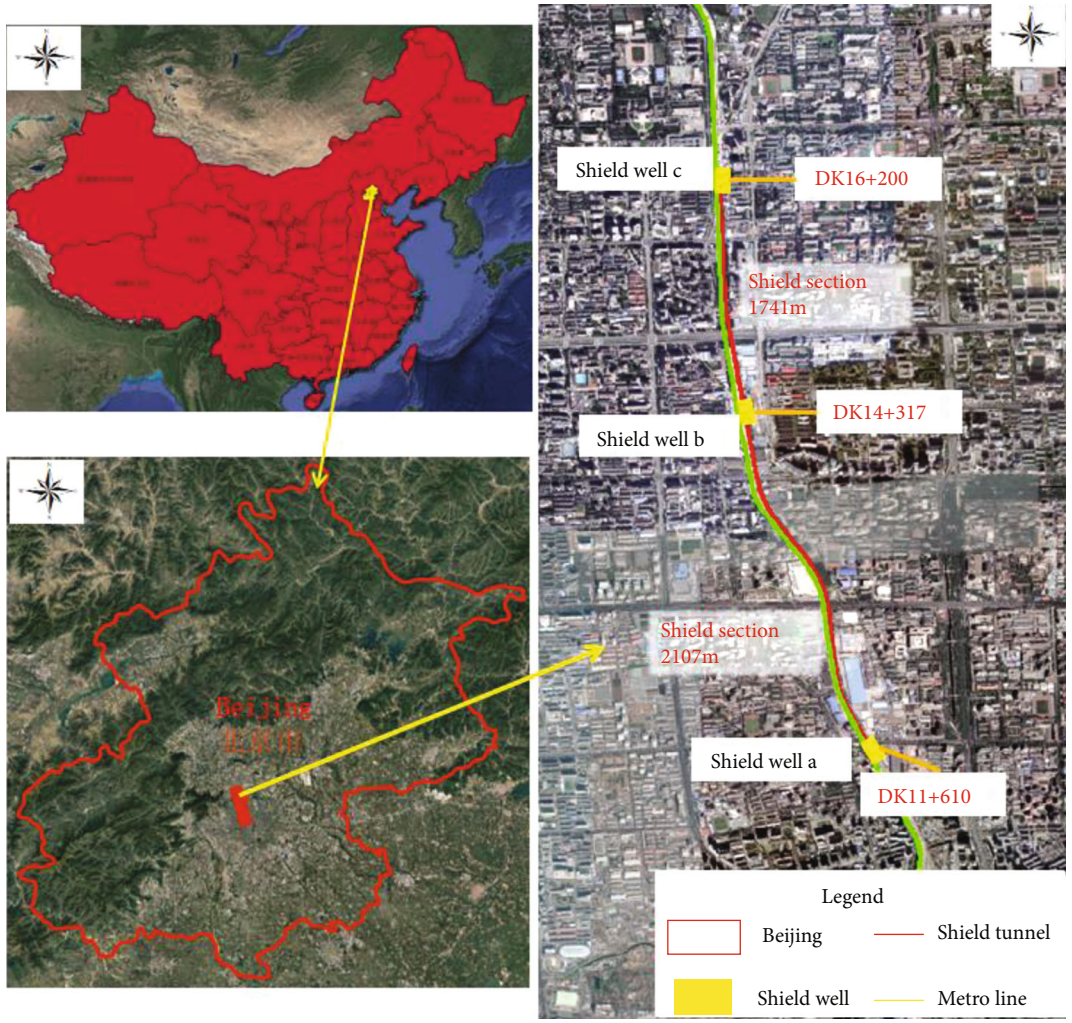

Figure 7: Position of the study area.

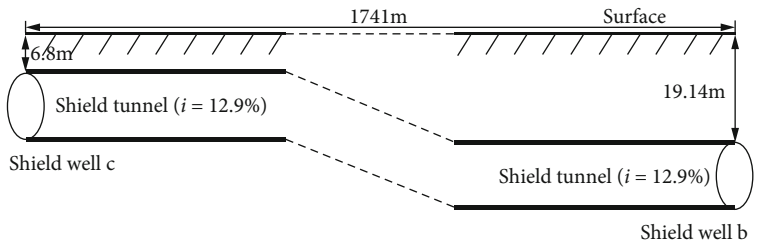

Figure 8: Longitudinal section of shield tunnel (between shield well b and shield well c).

can complement each other in monitoring ground subsidence caused by shield tunnel excavation. Figure 6 shows the processing workflow for deriving the ground movement parameters caused by the shield tunnel excavation using the two monitoring techniques. In order to fulfill the monitoring requirements (including monitoring accuracy, frequency, and coverage), a joint analysis is performed (InSAR and leveling), to derive the ground movement parameters. In addition, it is worth noting that two InSAR datasets (Sentinel-1 and CSK) used in this study have different wavelengths (i.e., C-band and X-band), which allow us to apply these data to monitor different regions based on the required monitoring accuracy.

3. Case Study

3.1. Study Area. As an important part of China's "eight vertical and eight horizontal" high-speed rail network, the Beijing-Zhangjiakou intercity high-speed railway, namely, the Beijing-Zhangjiakou high-speed rail, is an important transportation system for the Beijing 2022 Winter Olympics. The high-speed railway has a total length of 174 km and a

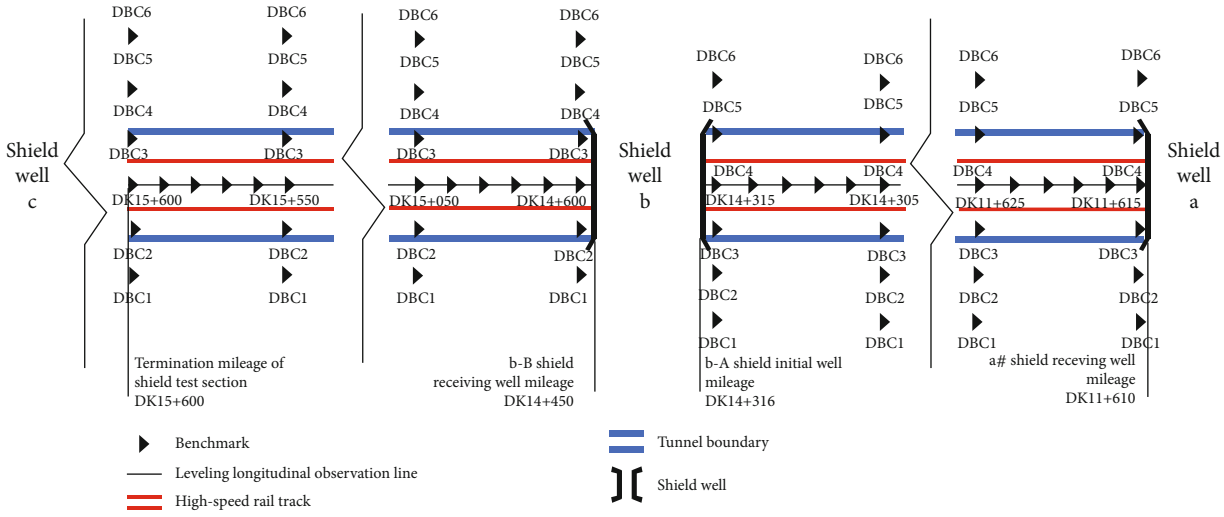

Figure 9: Plane layout of measuring points.

Table 2: Detailed characteristics information of Sentinel-1 and CSK dataset.

Satellite type	Imaging mode	Data band	Spatial resolution	Ascending/descending mode	Polarization mode	Number of images	Start time	Termination time
Sentinel-1A	IW mode	C-band (5.6 cm)	5 m × 20 m	A	VV polarization	28 scenes	20171210	20181123
COSMO-SkyMed	StripMap mode	X-band (3.1 cm)	3 m	D	HH polarization	38 scenes	20150129	20181106

Table 3: Acquisition date of the Sentinel-1 dataset.

Number	Date	Number	Date	Number	Date
1	2015/1/29	14	2016/6/24	27	2017/12/8
2	2015/4/23	15	2016/8/19	28	2018/1/6
3	2015/5/21	16	2016/9/20	29	2018/2/10
4	2015/6/22	17	2016/10/30	30	2018/3/11
5	2015/9/10	18	2016/12/2	31	2018/4/15
6	2015/10/12	19	2016/12/25	32	2018/5/1
7	2015/11/13	20	2017/2/4	33	2018/6/2
8	2015/12/19	21	2017/6/28	34	2018/7/4
9	2016/1/20	22	2017/7/1	35	2018/8/2
10	2016/2/9	23	2017/8/2	36	2018/9/3
11	2016/3/20	24	2017/9/16	37	2018/10/3
12	2016/4/13	25	2017/10/18	38	2018/11/6
13	2016/5/11	26	2017/11/6		

Table 4: Acquisition date of the CSK dataset.

Number	Date	Number	Date	Number	Date
1	2017/12/10	11	2018/4/21	21	2018/8/19
2	2017/12/22	12	2018/5/3	22	2018/8/31
3	2018/1/3	13	2018/5/15	23	2018/9/12
4	2018/1/15	14	2018/5/27	24	2018/9/24
5	2018/1/27	15	2018/6/8	25	2018/10/6
6	2018/2/8	16	2018/6/20	26	2018/10/18
7	2018/2/20	17	2018/7/2	27	2018/11/11
8	2018/3/4	18	2018/7/14	28	2018/11/23
9	2018/3/28	19	2018/7/26		
10	2018/4/9	20	2018/8/7		

total of 10 stations with a maximum design speed of 350 km/h. It is the world's first high-speed railway with a design speed of 350 km/h. The study area in this work is the DK11+610 (distance starting at the origin is 11610 m) to DK16+200 (16200 m) section of the Beijing-Zhangjiakou Railway, mainly located in Beijing (Figure 7). The total length of railway studied is around 4 km, and the railway adopts the shield construction method.

The shield tunnels pass through several main urban roads, such as the North Third Ring Road, Zhichun Road, and North Fourth Ring Road, and are adjacent to a certain subway line (Zhichun Road Station of Metro Line 10). The geology of shield tunnels is mainly pebble soil layer. The buried depth of the entrance end of shield well a and shield well c is about 7.0 m and 7.1 m, respectively. The buried depth is less than 0.6 times of the tunnel diameter, which belongs to an ultrashallow buried section. The stratum of the tunnel crossing the vault is dominated by mixed soil, silt, and silty clay. The end of the shield well a and the base stratum are dominated by silt and silty clay, with a little pebble soil in the middle. The end of the shield well c and the basement stratum are dominated by silty clay. The cave body and base stratum are mainly silty clay and pebble soil. The stratum has

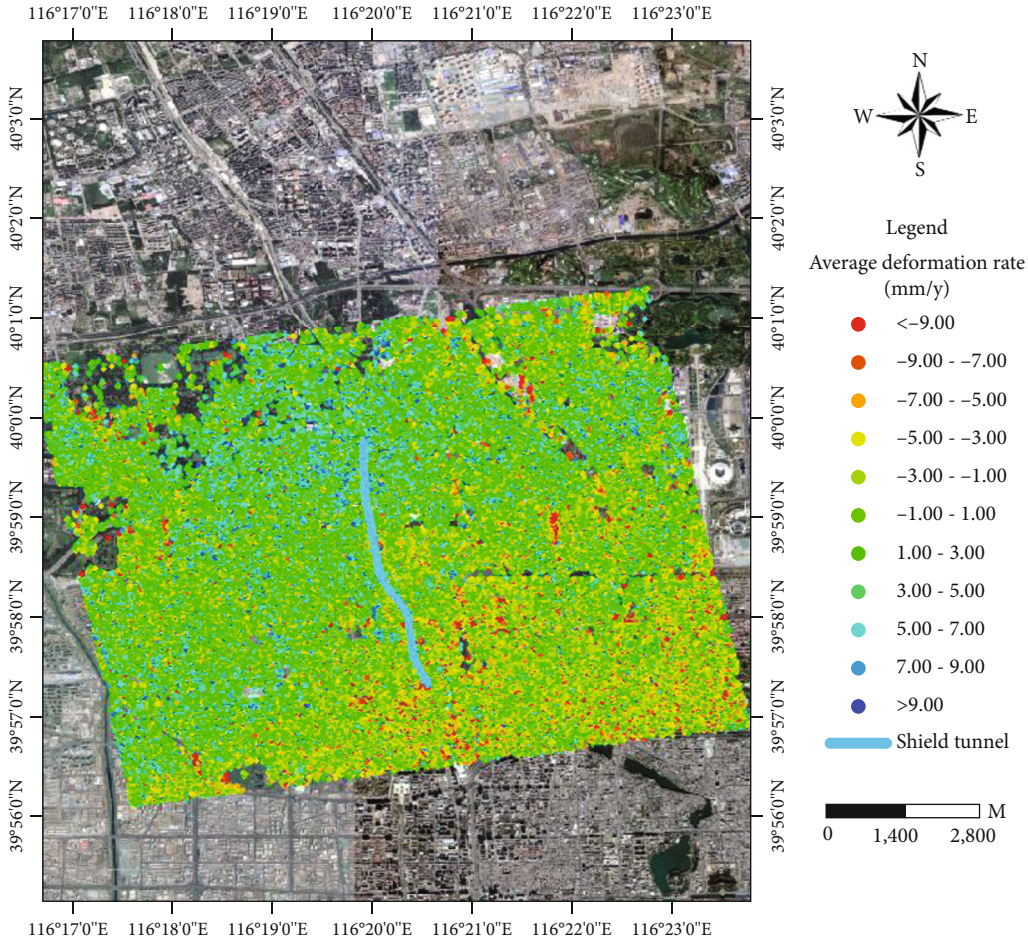

Figure 10: Average deformation rate map of Sentinel-1 from January 2017 to November 2018.

a large permeability coefficient, abundant groundwater, and poor bearing capacity of the stratum. The burial depth of the exit end of the shield well b is about 20 m, and the arch top stratum is dominated by clay, silt, fine sand, and silty clay. The cave body and base stratum are mainly composed of silty clay and pebble soil. The stratum has a large permeability coefficient, abundant groundwater, and poor bearing capacity of the stratum.

The shield tunnel passes through multiple sensitive old buildings, multiple water supply pipelines, sewage pipelines, heat pipe trenches, and high-pressure gas pipes where some sections are about 2 m away from the pipeline. The tunnel is also underneath a number of transport infrastructure, e.g., the North Third Ring Road, Zhichun Road, and North Fourth Ring Road frame bridge. In addition, a long section of the shield tunnel is parallel to Metro Line 13, for a distance of 4 stations along the line. The tunnel structure is relatively close to Line 13 (about 9.6 m-26.6 m). It also passes through the Zhichun Road Station of Metro Line 10, with the minimum clear distance of about 5.5 m from the structure. The shield tunnel process will affect the existing buildings (structure), pipelines, existing subways, or subways under construction. Therefore, during the process of shield tunnel excavation, it is necessary not only to carry out the control measurement and elevation measurement of the shield time and space but also to monitor the deformation of the ground surface and infrastructure, etc., to ensure that these objects are not affected by the shield tunneling or are within a controllable range before, during, and after the shield tunneling. Therefore, it is very important to comprehensively monitor the ground deformation caused by shield tunnel excavation.

The shield tunnel is assembled with fully prefabricated segments. The segments adopt outer diameter 12.2 m, inner diameter 11.1 m, ring width 2 m, and segment thickness 55 cm. It is divided into two shield sections, namely, the DK11+610 to DK14+317.5 section (the interval between shield well a and shield well b) and the DK14+459 to DK16 +200 section (the interval between the shield well b back and shield well c). A total of 3 shield wells are built, located at DK11+610 mileage (shield well a), DK14+317 mileage (shield well b), and DK16+200 mileage (shield well c), as shown in Figure 7. The distance between shield wells a and b is 2707 m. The railway line along the longitudinal direction is relatively flat at the beginning section; the slope was raised to 20° (downhill) after it enter the tunnels. The depth of the entrance and the exit of the tunnel is 21.4 m and 5.8 m, respectively, where the lowest point of the tunnel between wells a and b is 28.7 m. The section between shield wells b

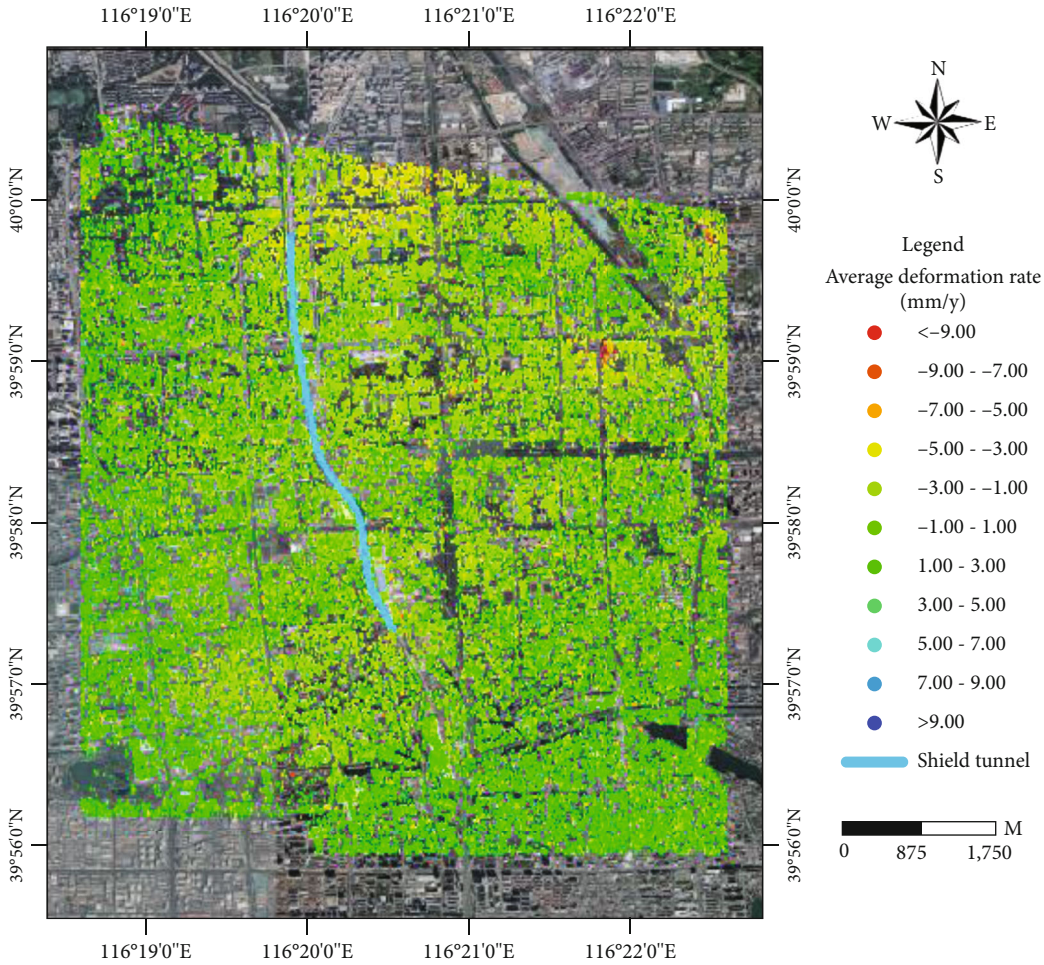

Figure 11: Average deformation rate map of CSK from January 2015 to November 2018.

and c is approximately 1741 m long. The longitudinal direction is also flat at the beginning section of b, where a slope of 12.9° (downhill) has been observed after entering the tunnel. The depth of the entrance and the exit of the tunnel is 6.8 m and 19.1 m, respectively, where the deepest point of the tunnel between wells b and c is located at the exit of the tunnel. Figure 8 shows the longitudinal section of the shield tunnel (i.e., the interval between shield well b and shield well c).

3.2. Leveling Data. When monitoring the tunnel excavation-induced ground subsidence near the centerline of the tunnel, the magnitude and rate of ground subsidence is expected to be high. The method of the leveling with flexible stations and high monitoring frequency should be used. Because the whole thread of the shield tunnel is long, the layout sketch map of the ground subsidence monitoring points is drawn to show the typical section (Figure 9). The leveling work is conducted daily, from 18 December 2017 till 25 November 2018, for shield sections a~b. The leveling work for shield sections b~c is conducted between 13 November 2017 and 25 October 2018. Since the shield line is too long, the project used a plane and leveling control network to ensure the consistency of the monitoring line [21, 24].

3.3. SAR Data. Twenty-eight Sentinel-1 data acquired from December 2017 to November 2018 and 38 CSK data acquired from January 2015 to November 2018 are used in this study. The detailed information of the two datasets is shown in Table 2. Tables 3 and 4 show the specific acquisition times of Sentinel-1 and CSK data.

3.4. InSAR Processing. The image acquired on 12 September 2018 and 04 February 2017 for Sentinel-1 and CSK dataset, respectively, is selected as the master image; all other images within the stack are interfered with the master image separately to generate the interferogram stack. The selection of the main image should ensure that the spatial baseline and the time baseline of each interference pair are the shortest, and the maximum average coherence coefficient can be obtained. The interferogram for each pair is generated using the 2-pass D-InSAR technique [25]. The SRTM DEM data (30 m resolution) is used to removing the terrain phase and the ground phase.

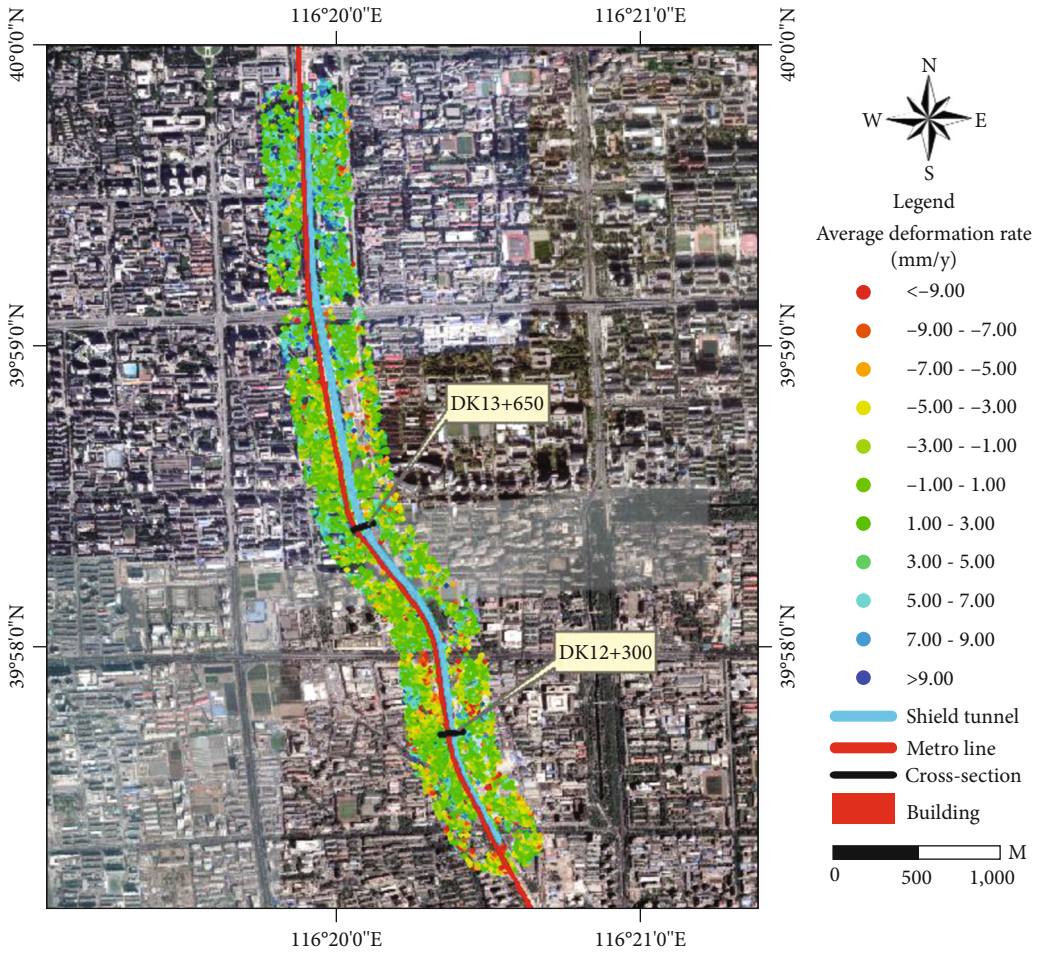

Figure 12: Average deformation rate map of Sentinel-1 shield section of Beijing-Zhangzhou high-speed railway from December 2017 to November 2018.

The TS-InSAR analysis in this work mainly follows the approach used in [8]. PS points in this work is determined using the amplitude dispersion index, which is calculated according to [8, 26]

$$D_A = d\frac{\sigma_A}{m_A}. \quad (1)$$

In Equation (1), σ_A represents the standard deviation of the coherence of the target point in N SAR images and m_A represents the mean of the coherence of the target point in N SAR images. The amplitude deviation threshold $D_{\text{Threshold}}$ is then applied to select the PS candidates. All pixels satisfying condition $D_A < D_{\text{Threshold}}$ are considered as PS candidates. According to the actual situation of the image data set and the study area, it is found that the best $D_{\text{Threshold}}$ value is 0.56 because it is able to maximize the number of final PS points without degrading the quality of the results.

After solving the linear deformation of each PS candidate point, the phase residual of the model is differentiated, low-pass filtering is performed in space, and a high-pass wave is applied to enough images in time. The filtering process takes into account the spatial and temporal correlation of atmospheric phase components. The low frequency component of phase residuals in time is related to the deformation component for modeling and should not be considered as an atmospheric effect.

After filtering, the atmospheric phase screen is estimated by Kriging interpolation on the regular image grid, and its variance map is taken into account, then the corresponding part is subtracted from each interferogram [27]. The nonlinear deformation components are obtained from the unwrapped residual phase after removing the linear displacement components and atmospheric artifact components from the original phase.

4. Results

4.1. TS-InSAR Results from Sentinel-1 Data and CSK Data. TS-InSAR results derived from the Sentinel-1 data and CSK data are shown in Figures 10 and 11, respectively. A total of 11806 and 27259 PS points, covering an area of about 1.6 km^2, fare obtained from the Sentinel and CSK data, respectively. These points are mostly located at the buildings, railways, and roads.

The TS-InSAR results show that the whole Beijing-Zhangzhou high-speed railway is relatively stable in general, but there is slight deformation obtained in some parts

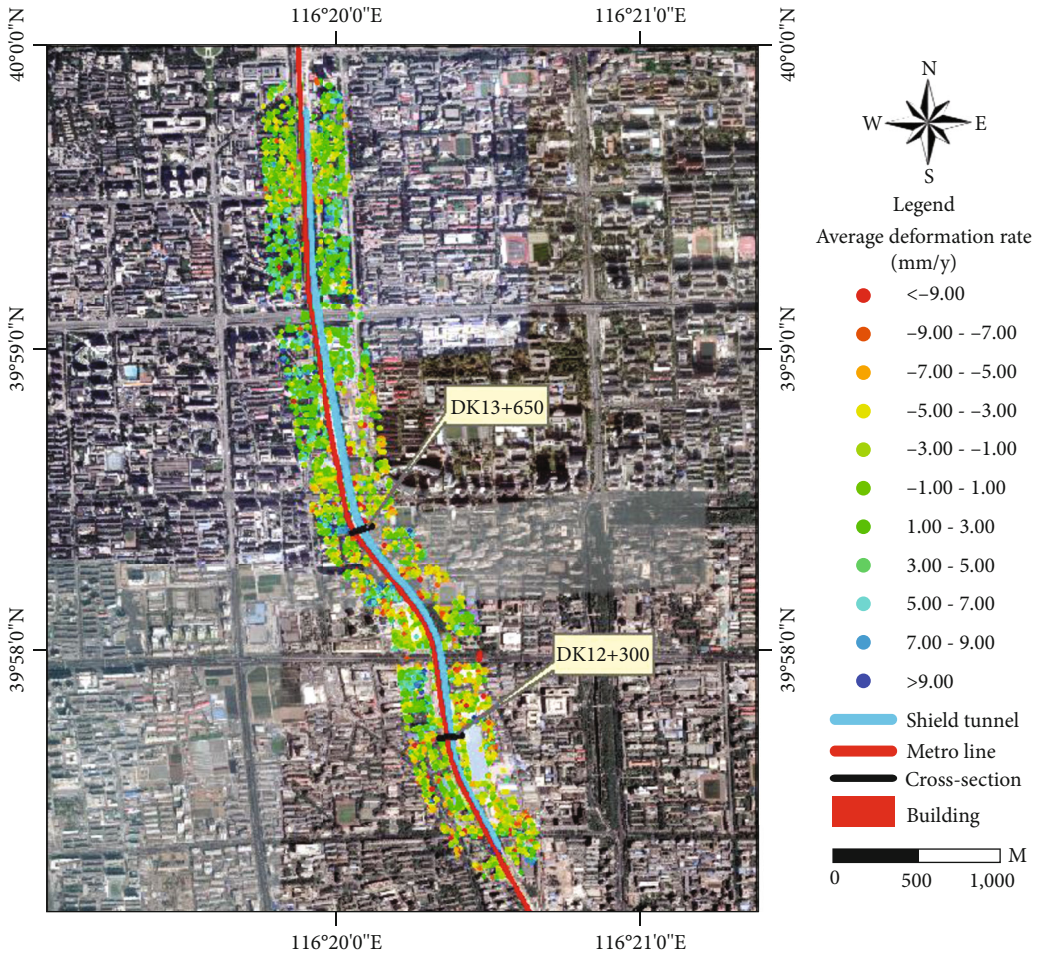

Figure 13: Average deformation rate map of CSK Beijing-Zhangzhou high-speed railway shield section from December 2017 to November 2018.

Table 5: Average advance influence angle and advance influence distance parameters of longitudinal section.

Shield tunneling interval	Average advance influence angle (°)	Average advance influence distance (m)
c~b	55.9	12.61
b~a	69.2	10.52

of the railway shield section. For example, there is obvious subsidence in the middle of the shield line, i.e., near the shield well b, but the overall subsidence is smaller.

As shown in Figures 12 and 13, the bottom picture is a satellite image of surface buildings near the shield tunnel. At the PS points on infrastructures, the points of different colors represent different subsidence of the PS points, as shown in Figures 12 and 13. And the number of CSK data obtained is obviously more than that of Sentinel-1. The local analysis of the results from the two datasets are as follows.

The difference in the number of PS points is because of the image resolution of Sentinel-1 data (5×20 m) which is poorer than CSK data (3×3 m). Because of the short wavelength from the CSK sensor together with the long spatio-temporal baselines in the CSK data stacks, the coherence of the ground targets other than the infrastructure is very low. But in densely built areas, the coherence of the buildings is high. The Sentinel-1 data has a longer wavelength and a

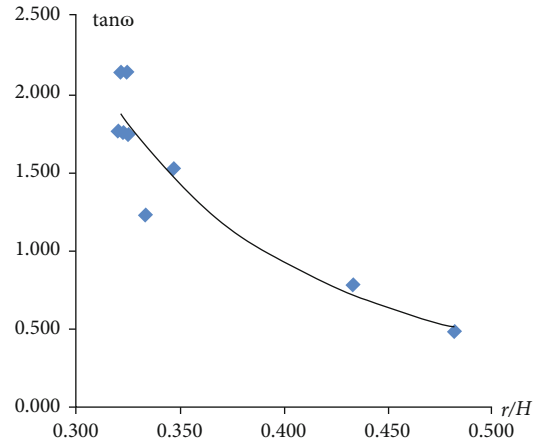

Figure 14: Relationship between the advance influence angle and the width-depth ratio of the tunnel.

Table 6: Average maximum subsidence velocity lag angle and lag distance parameters of longitudinal section.

Shield tunneling interval	Average advance impact angle (°)	Average leading influence distance(m)
c~b	64.3	8.75
b~a	60.1	14.73

shorter spatiotemporal baselines. Therefore, the Sentinel-1 data is more suitable for the monitoring of land subsidence over the nonbuilding areas.

4.2. Analysis of Ground Subsidence of Shield Tunnel

4.2.1. Advance Influence Angle in Longitudinal Section. According to the definition of the zone of influence and angle of influence, the influence distance and angle of two shield tunnels can be calculated by the leveling data. The average values of advance influence distance and angle of the two shield tunnels derived from the leveling data are shown in Table 5.

Based on the acquired advance influence angle, the relationship between the advance influence angle and the shield excavation depth is shown in Figure 14.

The relationship between the tangent value of advance influence angle and the width-depth ratio of shield tunnels is expressed by

$$\omega = \tan^{-1}\left[0.05\left(\frac{r}{H}\right)^{-3.2}\right], \quad (2)$$

where r is the outside radius of shield tunnel segment.

According to the structural information of the shield tunnel, it is known that the outside radius r is a fixed value. From the functional relationship between the advance angle of influence of the shield tunnels and the ratio of the width to depth of the tunnels, it can be seen that the advance angle of influence of the shield tunnels increases with the increasing depth of the shield tunnels.

4.2.2. Lag Distance and Lag Angle of Maximum Subsidence Rate. The lag angle and lag distance of the average maximum subsidence rate of the two sections of the shield tunnel are obtained from the leveling measurements (Table 6). Different lag distance and angle between the two sections of the shield tunnels have been observed. This is expected to be because of the difference in shield tunnel depth and shield speed.

Based on the lag angle data derived from the leveling measurement, it is possible to derive the relationship between the lag angle and the shield tunnel, as shown in Figure 15.

The function expression of the lag angle and tunnel width-depth ratio is

$$\varphi = \tan^{-1}\left[0.16\left(\frac{r}{H}\right)^{-1.8}\right]. \quad (3)$$

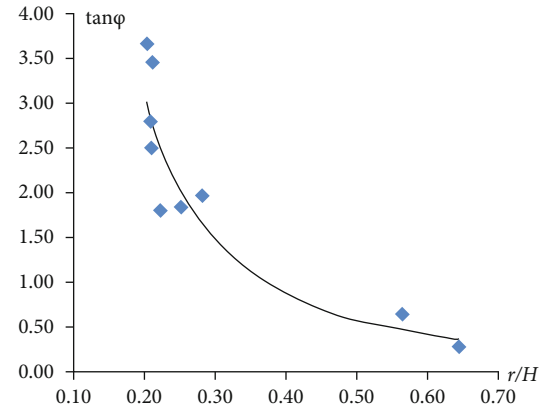

Figure 15: Relationship between lag angle and width-depth ratio of shield tunnels.

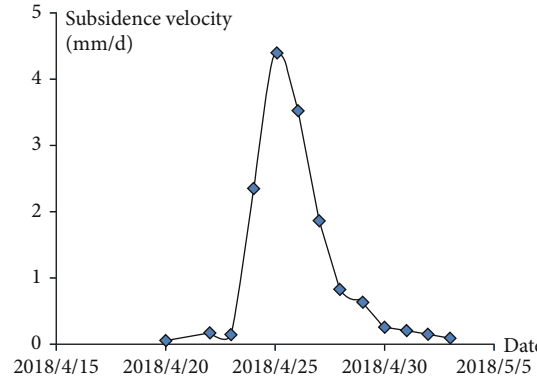

Figure 16: Variation of subsidence rate of upper surface point at the deepest position of tunnel midline.

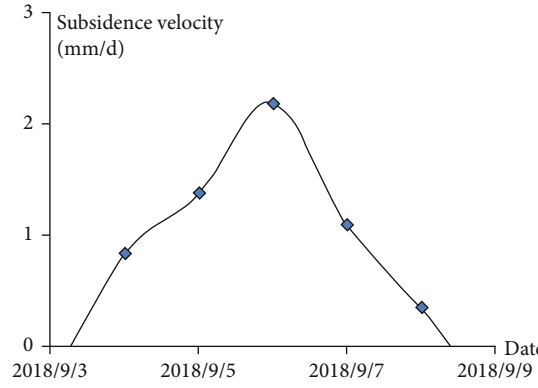

Figure 17: Variation of subsidence rate of a shallow upper surface point along the middle line of tunnel.

The lag angle of the shield tunnel decreases with the decrease of the depth of the shield tunnel. By understanding the effect of variation in the lag angle to the maximum ground subsidence rate, it is possible to determine the high-risk area from different shield working faces. This information is of great significance for the protection of the ground surface of shield tunneling.

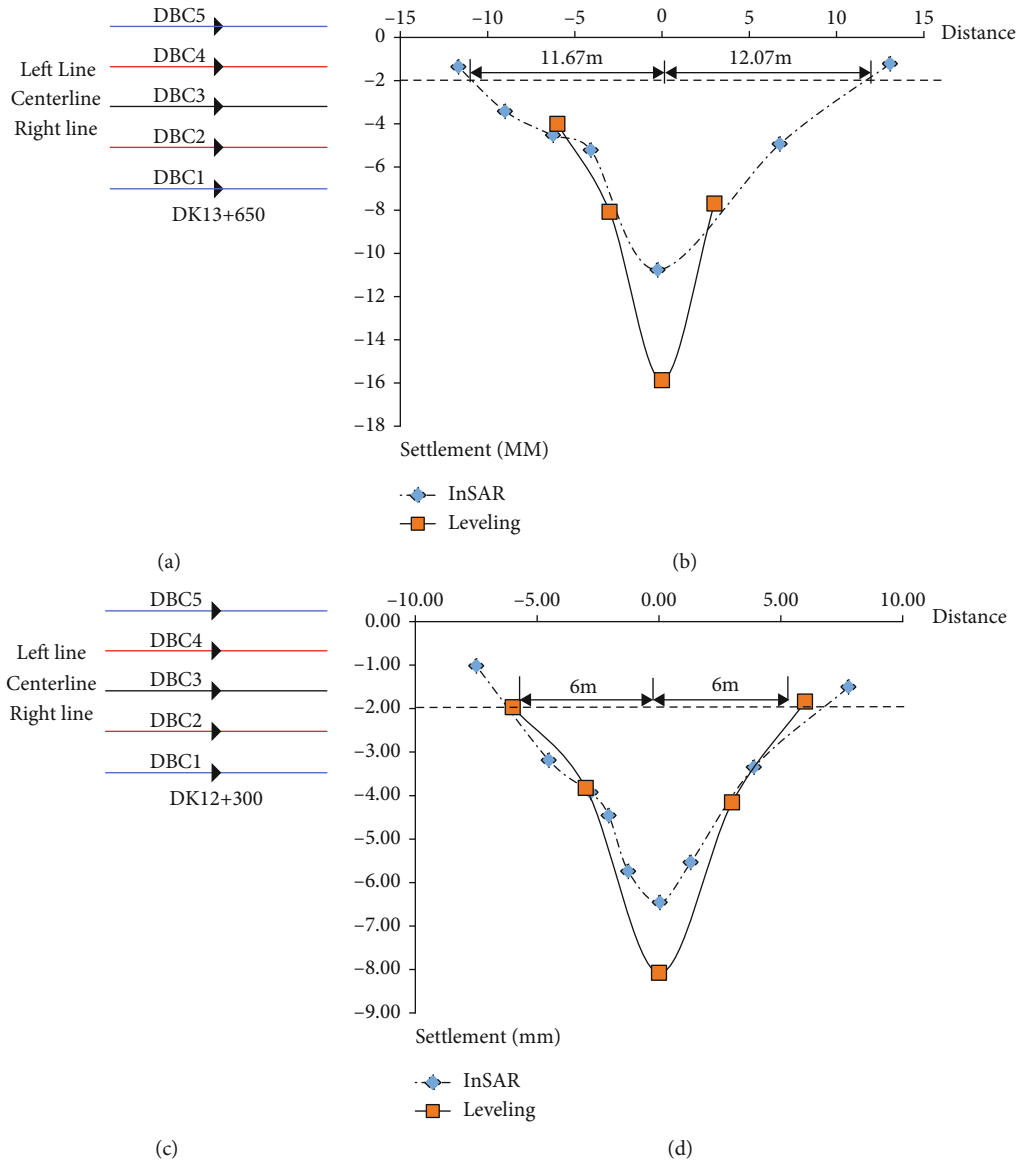

Figure 18: Leveling point layout and transverse influence distance: (a) DK13+650 cross-section leveling point layout; (b) DK13+650 transverse influence distance; (c) DK12+300 section leveling point layout; (d) DK12+300 transverse influence distance.

4.2.3. Surface Subsidence Time Determination of Shield Excavation. Due to the limitation of the monitoring frequency, the leveling is chosen to obtain the surface subsidence time determination of shield excavation since this method can achieve the observation frequency of once a day. In this work, the variation of the subsidence rate at the deepest part of the middle line of the shield tunnel (tunnel depth 29.95 m) and at the shallow part of the tunnel (tunnel depth 9.5 m) is described in Figures 16 and 17, respectively.

During the shield tunneling process, the subsidence rate of the surface point changes regularly: (1) the initial subsidence rate changes slowly, with the advance of the shield plane; (2) the subsidence rate increases gradually, reaching the maximum value; (3) the subsidence rate decreases gradually until the surface movement stops.

Table 7: Cross-sectional influence boundary angle results.

Cross-section number	Transverse influence distance (m)	Maximum subsidence of middle line of tunnel (mm)	Tunnel depth (m)	Lateral influence on boundary angle (°)
DK13 +650	Left 11.67	-15.87	29.92	68.7
	Right 12.07			68.0
DK12 +300	Left 6.00	-8.08	10.45	60.1
	Right 6.00			60.1

Based on the subsidence measurements along the Beijing-Zhangzhou high-speed railway, it is possible to investigate the subsidence rate variation patterns caused by tunneling at different depths. As described in the two pictures above, for deep tunnels, it can be found that the subsidence

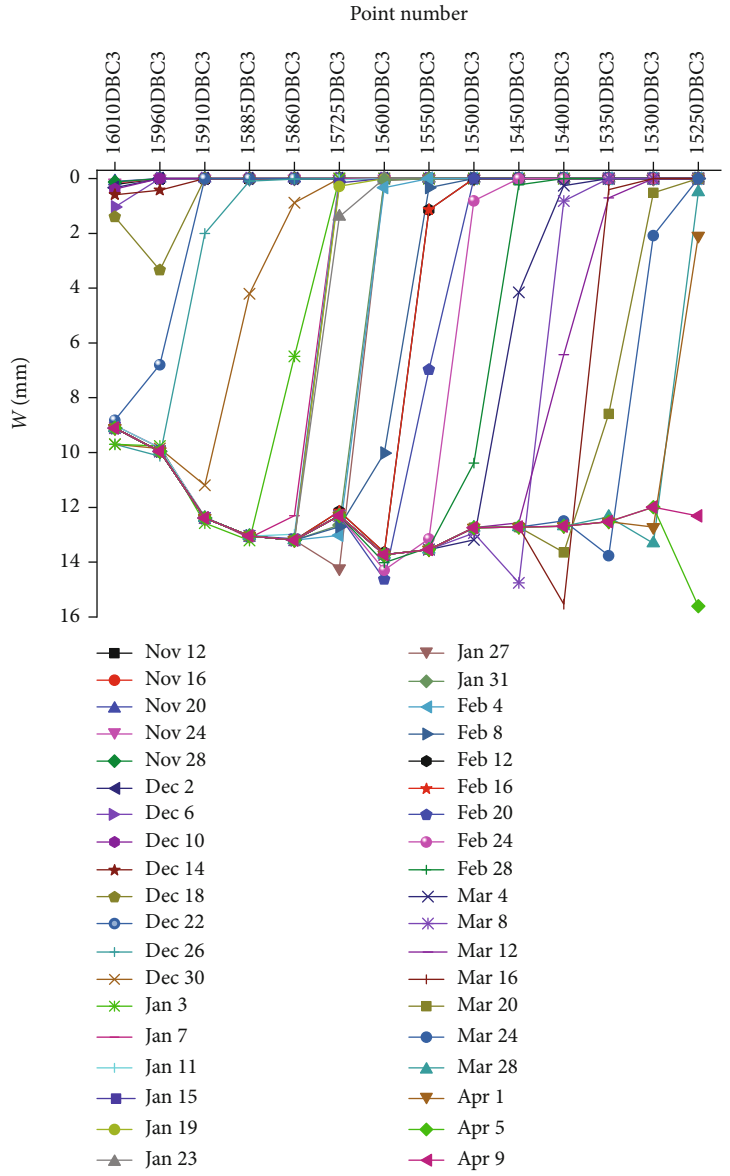

Figure 19: Dynamic sinking curve diagram of shield tunnel centerline.

rate takes about two days from 0 to 1 mm/day, it then takes another two days to reach to the maximum subsidence rate, and then it takes another eight days for the subsidence rate to go back to 0 mm/day. For the shallow tunnels, it takes one day for subsidence rate to reach 1 mm/day, then it takes another two days to reach the maximum and takes another three days to go back to 0 mm/day. The results show that the time for surface movement caused by excavation of deep and shallow tunnels in Beijing-Zhangzhou high-speed railway shield tunnels is 12 days and 6 days, respectively. Understanding the variation of subsidence rate caused by shield tunneling at different depths has practical significance for the protection of the ground surface and buildings above the shield tunneling, as the time range of rapid ground surface movement during shield tunneling can be determined.

In this paper, whether it is a deep tunnel (29.95 m) or a shallow tunnel (9.5 m), the duration of surface movement is within 12 days. According to the above results, the determination of the continuous surface movement time requires a high-time flat rate (once a day) and high-precision ground subsidence monitoring. Due to the time period of satellites visiting the same area and the high time frequency of leveling, it is suitable for us to use leveling to obtain the duration of surface movement and make regular analysis.

4.2.4. Determination of Influence Distance in Transverse Direction Using InSAR. The InSAR technique has the capability of mapping deformation with wide coverage, which can be used as a supplement technique for determining the influence ground surface distance in the transverse direction of the shield tunnel axis. In this study, a monitoring cross-section profile near the deepest burial depth of the shield tunnel (DK13+650) and a cross-section profile at the shallower

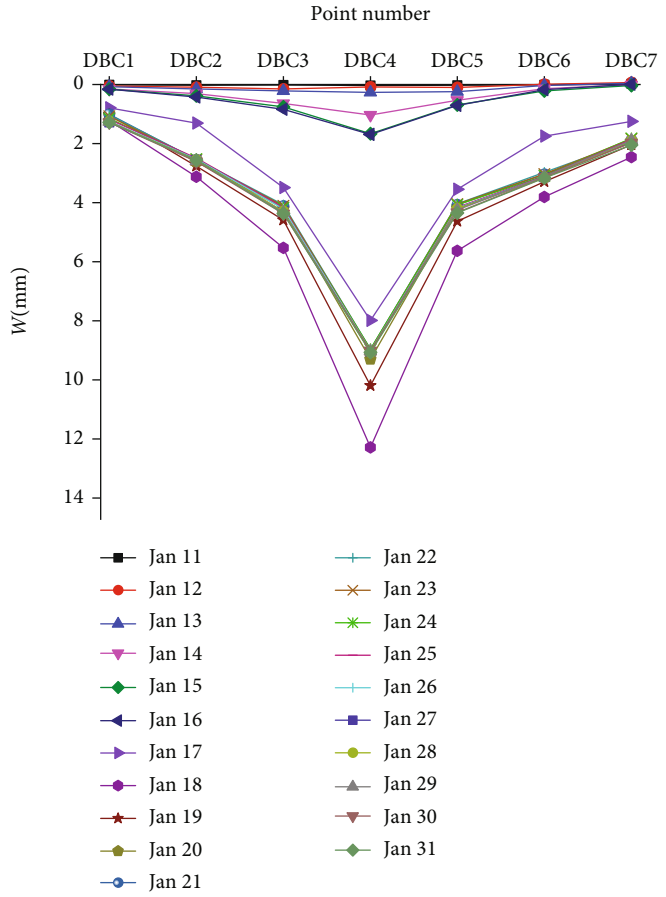

Figure 20: 15795 cross-section subsidence curve.

burial depth of the shield tunnel (DK12+300) are selected for analysis.

The layouts of cross-sectional DK13+650 and DK12+300 leveling points are shown in Figures 15(a) and 15(c), respectively. Taking the middle line of the tunnel as the center, the distance between the survey points on the right side and the middle line of the tunnel is defined as negative values, and the distance between the survey points on the left side and the middle line of the tunnel is defined as positive values. The TS-InSAR measurements and the leveling measurements of the tunnel cross-section is shown in Figures 18(b) and 18(d) for DK13+650 and DK12+300, respectively.

Taking 2 mm as the transverse influence boundary [23], it can be determined that the influence ranges of the left and right sides of the tunnel middle line at DK13+650 section are 11.67 m and 12.07 m, respectively, and the DK12+300 section counterpart are 6 m on both sides. The results agree well with the theory about the influence of underground activities on the ground surface, i.e., the deeper the buried depth, the larger the influence range of the surface.

InSAR obtain the deformation along the LOS direction of the satellite, while the ground subsidence obtained by leveling is in the vertical direction. As a result, the difference between the target points of InSAR measurements and the leveling measurements appears, and the maximum subsidence value of InSAR results is slightly different from that of the leveling monitoring results. The maximum surface subsidence and cross-section influence boundary obtained from leveling and InSAR data are used to calculate the lateral influence boundary angle of the shield tunnel surface (see Table 7). The results show that the boundary angle of the transverse movement of the surface of shield tunnel is between approximately 60 and 70°.

4.3. Analysis of Subsidence of Buildings Near the Shield Tunnel. Since it is not possible to directly measure the subsidence of the buildings near the shield tunnel, the subsidence of the ground surface at the side of the buildings is studied instead. The subsidence obtained at these areas is expected to reflect the subsidence of the buildings. Figure 19 shows the subsidence value of different leveling monitoring points from 12th November 2017 to 5th April 2018. In Figure 19, the abscissa represents the monitoring points on the center of the shield tunnel in the longitudinal direction. As the tunnel excavation advanced, the ground subsidence influence range gradually expands, and the maximum ground subsidence gradually increases before being stabilized.

According to the depth of shield tunnel excavation, three cross-sections of the shield tunnel are selected for analysis. The corresponding excavation depths of the three cross-

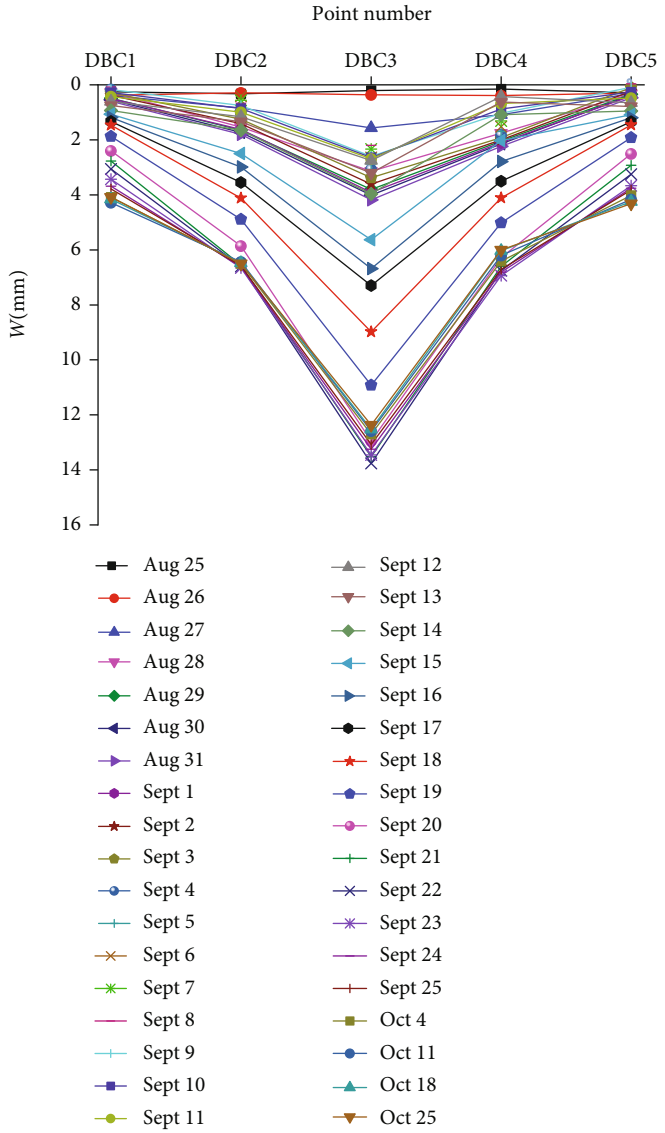

Figure 21: 14460 cross-section subsidence curve.

sections (15795, 14460, and 13600) are 12 m, 19 m, and 29 m, respectively. As shown in Figures 20–22, the abscissa is the leveling monitoring point of the cross-section, and the ordinate is the corresponding subsidence value. The maximum surface subsidence points on the three cross-sections are the tunnel midline points, and the maximum subsidence is 14.2 mm, 13.76 mm, and 14.64 mm, respectively. The overlying surface subsidence curve of the shield tunnel is approximately symmetrical, with the maximum subsidence value appearing above the tunnel centerline; the subsidence value (maximum subsidence value) of the leveling monitoring points gradually decreases to zero as they become further away from the shield tunnel centerline. During the shield tunnel excavation, (1) the subsidence value of the surface monitoring points slowly increased, (2) the magnitude of the subsidence rapidly increased, (3) the surface rebounded slightly upwards because of the lining support, and (4) the subsidence value tends to stabilize. The surface subsidence values of the three cross-section tunnels after the centerline is stabilized are 10.48 mm, 12.37 mm, and 10.91 mm.

Figures 23 and 24 shows the deformation rate and cumulative deformation along the existing metro line L1. Figure 25 shows the accumulated historic deformation change map of metro line L1. Metro line L1, which runs on the surface, is parallel to the tunnel shield. Because of the influence of the satellite looking angle, intensive infrastructure, and construction works, lack of PS points has been observed in some sections along the metro line (mostly between approximately b and a shield tunnels). Therefore, the analysis work is focused on analyzing the deformation between approximately c and b shield tunnels.

There are 1599 PS points observed in this section, of which the deformation rate of 11.4% (182) of them is greater than 8 mm/year. The maximum rate observed is 16.5 mm/year, which is located on the subway line west of the shield well b. There are 43 (2.1%) PS points with the

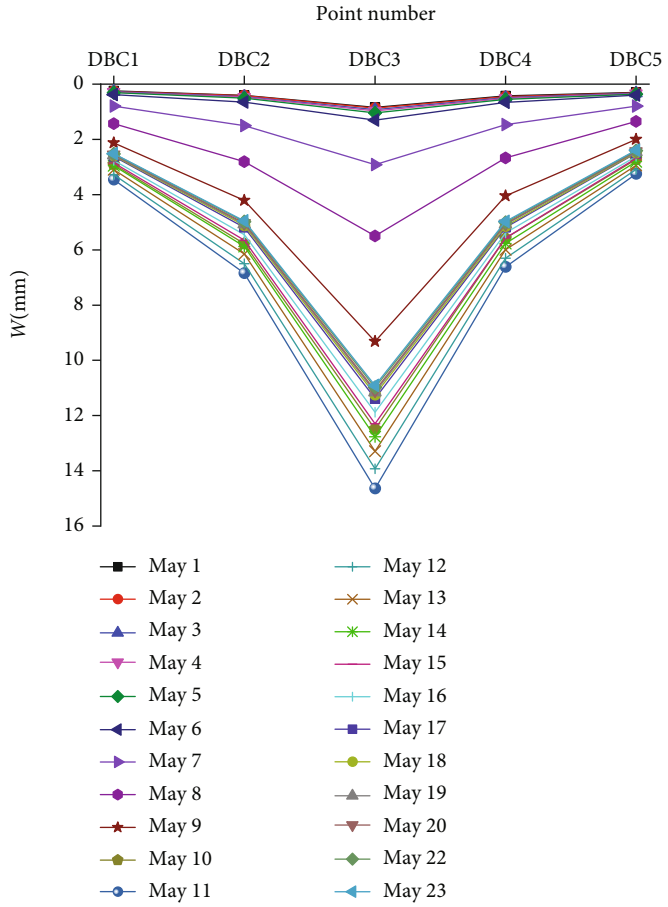

Figure 22: 13360 cross-section subsidence curve.

accumulated deformation value exceeding 10 mm, which are mainly located in the west of the starting point of the shield well b.

From December 2017 to March 2018, the accumulated deformation of the metro line is within ±5 mm, where most of the deformation areas are near the shield shaft. By June 2018, the accumulated subsidence of some areas, especially near shield well b, is over 9 mm. The overall deformation of the metro line (Figure 26) near the shield well b has become stable between March 2018 and November 2018. The historical accumulative deformation data shows that the underground excavation of the tunnel has little or no effect on the metro line L1. However, it has been observed that the excavation of the shield shaft has certain effects on the metro line L1. This is because the size and depth of the shield shaft are larger than those of the shield tunnel, so the influence area is relatively larger.

The distance between the shield well b and the parallel metro line (i.e., L1) is about 29-32 m, and the historical subsidence of the metro at the start-up well of shield B is shown in Figure 27.

Based on the deformation rate of the PS point observed along the metro line L1, the excavation of shield tunnels has certain impacts on the nearby metro line L1; continuous deformation has been observed for 8 months. The deformation is not obvious in the initial stage, while the deformation issue between March and May 2018 is relatively stable. However, the subsidence has accelerated after May 2018.

Shield tunnel excavation can have impact on the ground surface, especially on the surrounding buildings. Understanding of the tunnel excavation impact on surrounding buildings in a timely manner is therefore very important for providing technical support for shield construction. InSAR technology, with large spatial coverage, is used here to monitor the surrounding construction of tunnels.

The influence of the shield tunnel excavation on nearby buildings of the Beijing-Zhangzhou high-speed railway is investigated by analyzing the deformation of a few buildings selected near the shield tunnel.

4.3.1. Building A (About 13 m Away from the 19 m Deep Tunnel Section). The displacement time series of the PS point on the building is shown in Figure 28. The building was stable before July 2018, then the subsidence of building A began after July 2018. The subsidence rate has accelerated rapidly after September 2018. The total deformation at this location was about 10 mm by November 2018. According to the shield tunnel excavation schedule, the construction work of the tunnel section near the inspected building is 1 August 2018, which coincides with the time of the building deformation.

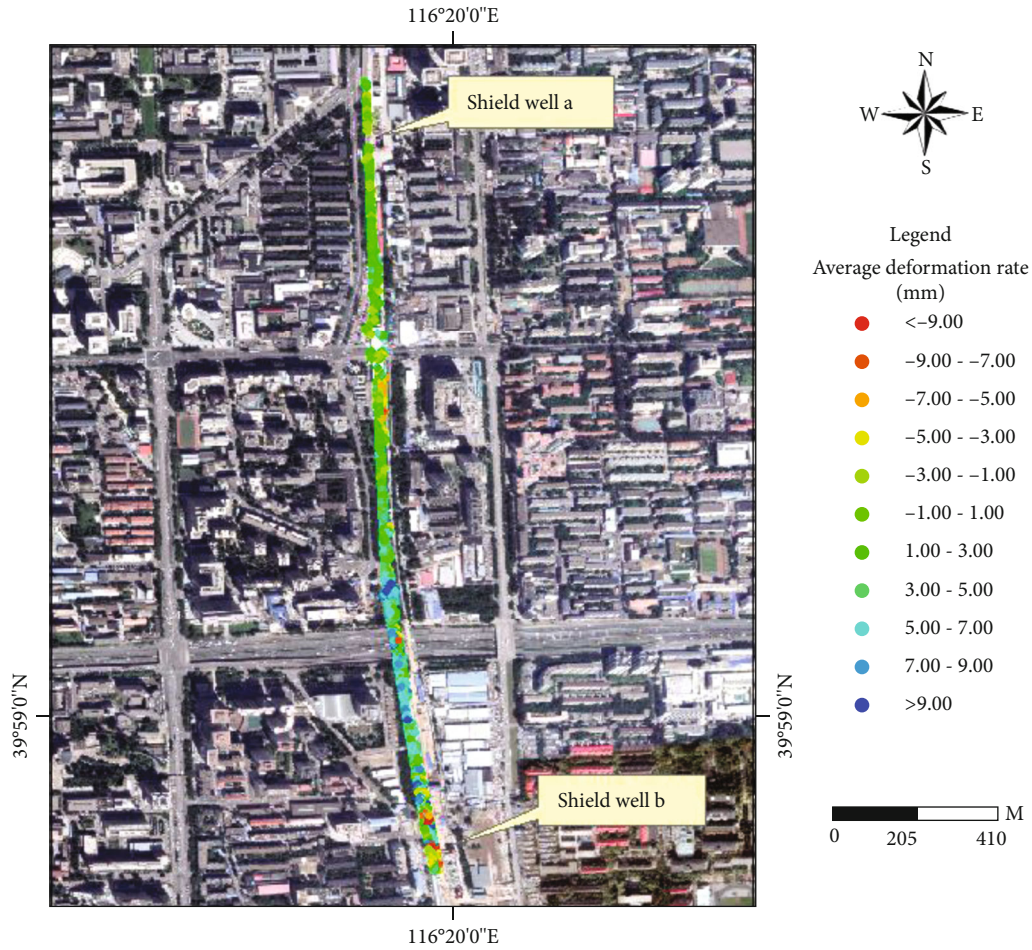

Figure 23: Annual deformation rate map (CSK) of metro line L1 from December 2017 to November 2018.

4.3.2. Building B (About 12 m Away from the 29 m Deep Tunnel Section). The displacement time series (Figure 29) show that the subsidence of the building began after March 2018 and tended to be stable after June 2018. The total subsidence value is about 5 mm between these periods. The subsidence rate between June and October 2019 was greatly reduced with subsidence of only 1 mm. According to the excavation schedule of the shield tunnel, the construction of this section began in mid-March 2018. This agrees with the InSAR results well, as it can be found that there is an obvious subsidence phenomenon between March and April 2018.

4.3.3. Building C (About 15 m–28 m Away from the 29.3 m Deep Tunnel). Figure 30 shows the deformation time series of the PS points at a building 15 m and 28 m away from the tunnel. Although a similar deformation trend has been observed at the two points, the point near the tunnel begin to deform earlier than the point further away. In addition, the coherence of the deformation of the point that is near is larger than that of the point that is far away. The shield tunnel excavated works at this section began in early April 2018, where the deformation rate of the two PS points between March and April is obviously larger than other periods.

4.3.4. Building D (12.5 m Away from the 10.5 m Deep Tunnel). Figure 31 shows that the deformation of the point is relatively stable from December 2017 to July 2018, and the subsidence occurs from July 2018. The deformation rate has gradually increased from July 2018, with total deformation of 9 mm observed by November 2018. The shield tunnel excavation at this section began at the end of August 2018, which coincides with the deformation trend observed at the building.

4.3.5. Building E (33 m Away from the 7 m Deep Tunnel). Figure 32 shows that the subsidence began in December 2017, and there is fluctuation between January 2018 and November 2018. The overall subsidence is about 3 mm. The shield tunnel excavation at this section began in early September 2018. The displacement time-series results show that the subsidence phenomenon began in December 2017, which does not coincide with the shield tunnel excavation schedule. Given that the coherence of the overall deformation is small, there is no evidence suggesting that the building is affected by the excavation.

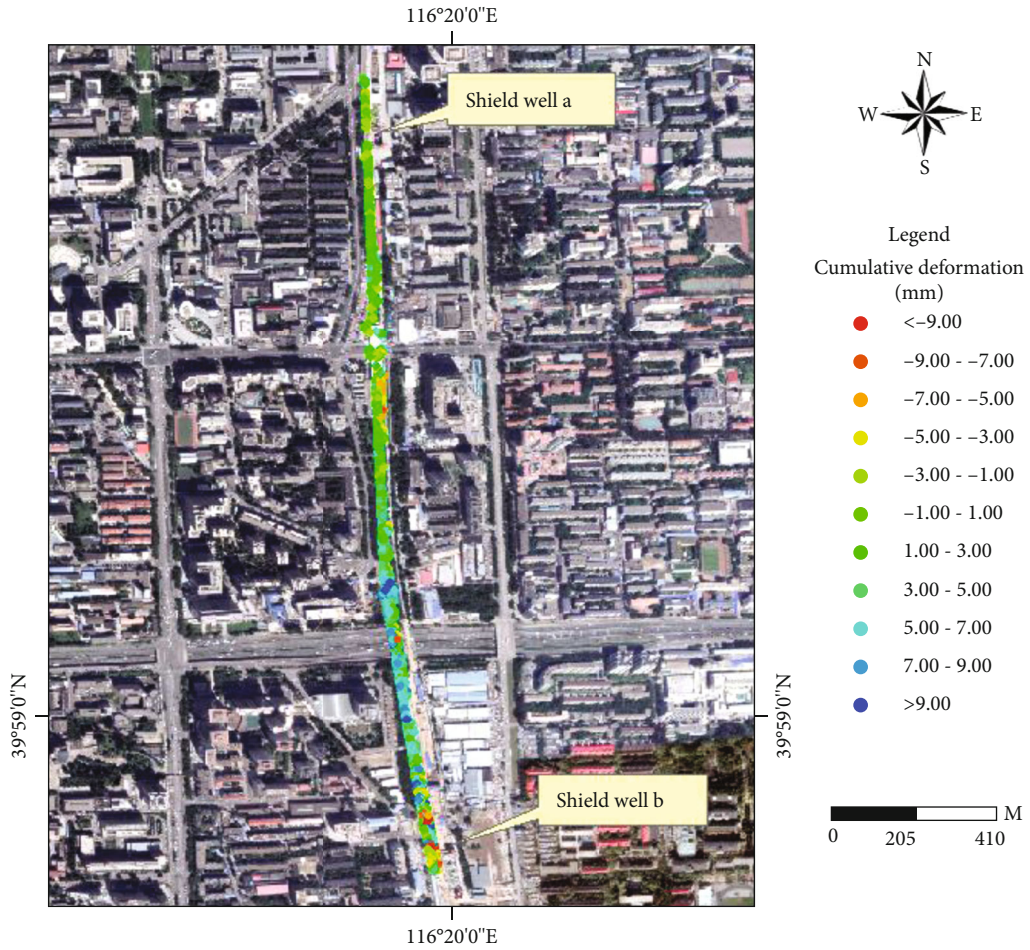

Figure 24: Accumulated deformation map (CSK) of metro line L1 from December 2017 to November 2018.

Together with the excavation schedule of shield tunnels, the deformation of buildings with a different distance along the shield tunnels is investigated. The results show that the impact to buildings is influenced by the depths of the tunnel. Moreover, the buildings around shield tunnels will take a long time to change stability. In order to ensure the safety and effectiveness of underground activities, it is necessary to monitor the infrastructure near the underground activities. The effectiveness of InSAR for monitoring deformation of surface infrastructures caused by underground activities is demonstrated in this work.

5. Discussion

In this study, taking full account of advantages and disadvantages of multiband InSAR and leveling in monitoring shield tunnel excavation caused by ground surface deformation, a joint monitoring method was established to study the deformation law of the overlying surface during the process of shield tunnel excavation. The surface movement multiband InSAR large-area monitoring and high-frequency and high-precision leveling were established to study the deformation law of the overlying surface during the process of shield tunnel excavation. The leveling measurement method is flexible to monitor the surface deformation at the selected point with high accuracy and frequency (e.g., on a daily basis). For example, when determining the duration of surface movement, the InSAR measurement is limited by satellite access cycle (varies from days to months), which is not ideal for monitoring the total movement time of ground subsidence (typically 6-12 days). Therefore, the use of leveling measurement is preferred in this case. When studying the deformation characteristics of buildings on the shield tunnel that is with some distance away from the tunnel line, it is required to obtain the continuous measurement with large spatial coverage and long time span. In such a case, InSAR is more suitable. X-band CSK data has a shorter wavelength and higher resolution than the C-band Sentinel data. Therefore, when monitoring the surface deformation caused by shield tunnel exaction, the X-band CSK data is more suitable for monitoring the deformation of houses near the shield tunnel, while the C-band Sentinel data is preferred for monitoring the deformation of nonbuildings near the tunnel. In summary, leveling data can be used to obtain the surface deformation-related parameters, such as lag distance and lag angle of the maximum subsidence rate, advance influence angle in the

Figure 25: Accumulated historic deformation change map (CSK) of L1 metro line.

longitudinal section, and surface movement duration; InSAR measurement can be used to obtain the information in large areas (e.g., buildings and nonbuildings near the tunnel) to determine the surface subsidence range on the cross-section of tunnel excavation direction as well as the influence angle of the subsidence boundary to from the shield tunnel. Based on above methods, a joint monitoring model of ground subsidence caused by shield tunnel excavation was established.

Based on the above-mentioned joint monitoring, the excavation-induced surface deformation can be dynamically monitored all around, with a long time span, and over a large area. In this article, it can be found that during the tunnel excavation, the advance influence angle of the tunnel surface subsidence increases with the increases of the shield tunnel depth, and the lag angle of the maximum subsidence rate increases with the increase of the tunnel excavation depth. These two parameters have related fitting formulas with the tunnel excavation depth. The leveling results suggested that the greater the excavation depth, the longer the subsidence duration. When using the multiband InSAR to monitor surface buildings and nonbuildings, it was found that the ground surface of the buildings and nonbuildings near the tunnel was relatively stable. The noticeable sinking areas identified were mainly concentrated near the centerline of the shield tunnel. The amount of subsidence decreases rapidly from the centerline of the tunnel to the left and right sides (i.e., transverse direction).

Through the above-mentioned joint monitoring of the shield tunnel excavation deformation model, the factors such as depth of the tunnel excavation, the influence distance in transverse direction, the characteristics, and the laws of ground subsidence during the shield tunnel excavation are obtained. At the same time, the surface movement parameters obtained by the authors using the framework show that when the shield technology is applied to tunnel excavation, it can effectively control the surface deformation. Once the surface deformation is under control, the risk of building deformation caused by surface deformation can also be reduced, and the probability of other land deformation-related disasters such as surface water and faults can be minimized. The safety of people's lives and property can hence be effectively protected, and the natural environment around the shield tunnel has also been successfully protected.

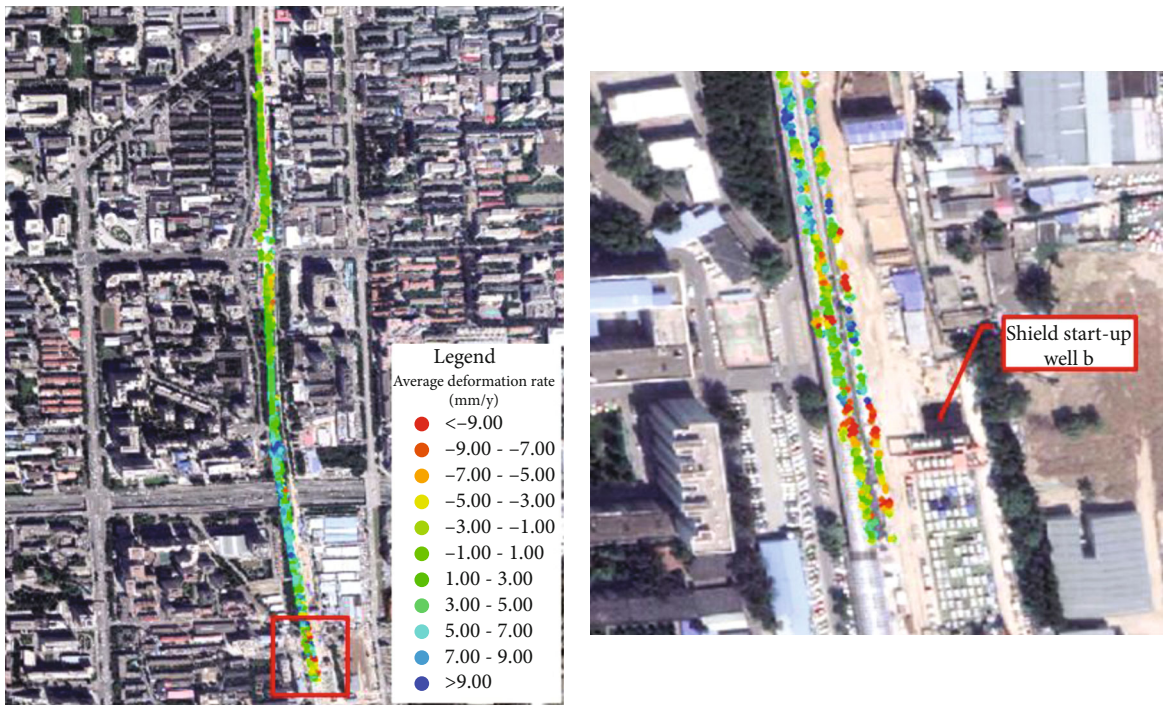

Figure 26: Deformation of metro line L1.

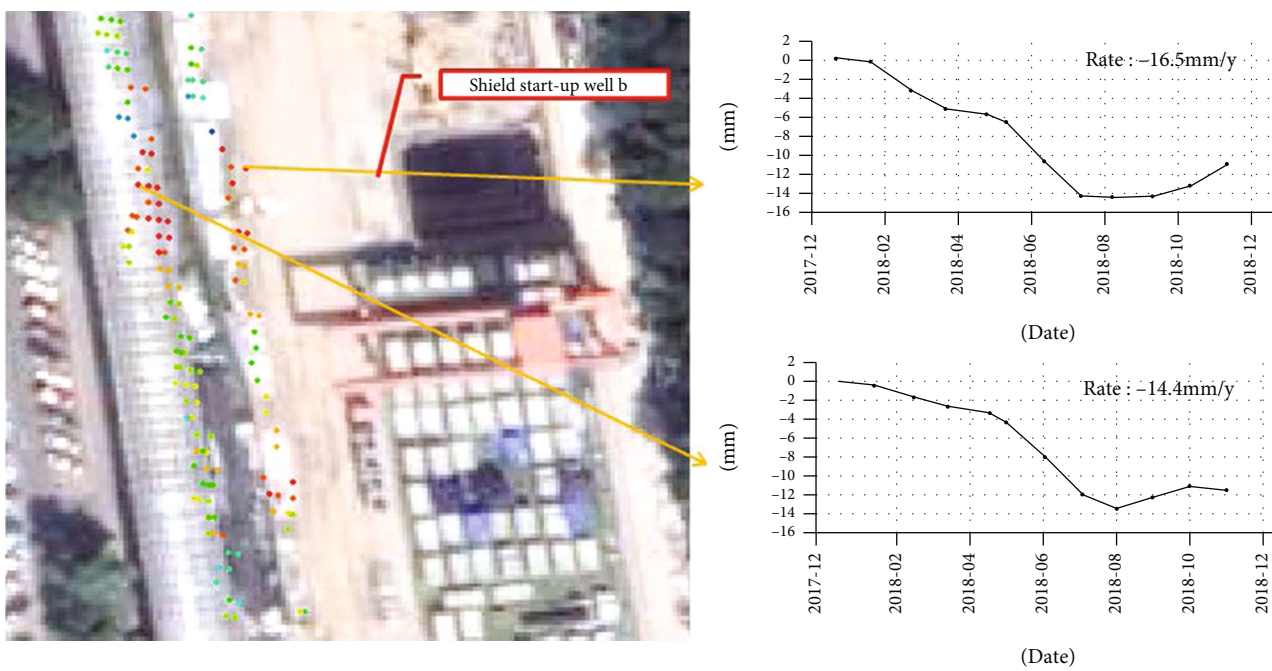

Figure 27: Historic deformation of PS point on metro line L1.

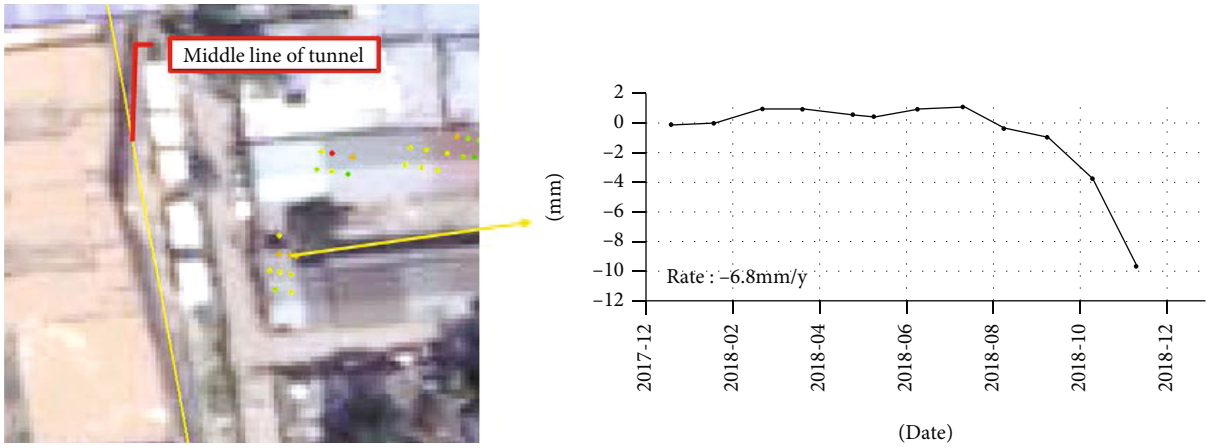

Figure 28: Position relation between building A and the middle line of the tunnel and the displacement time series of a PS point on the building.

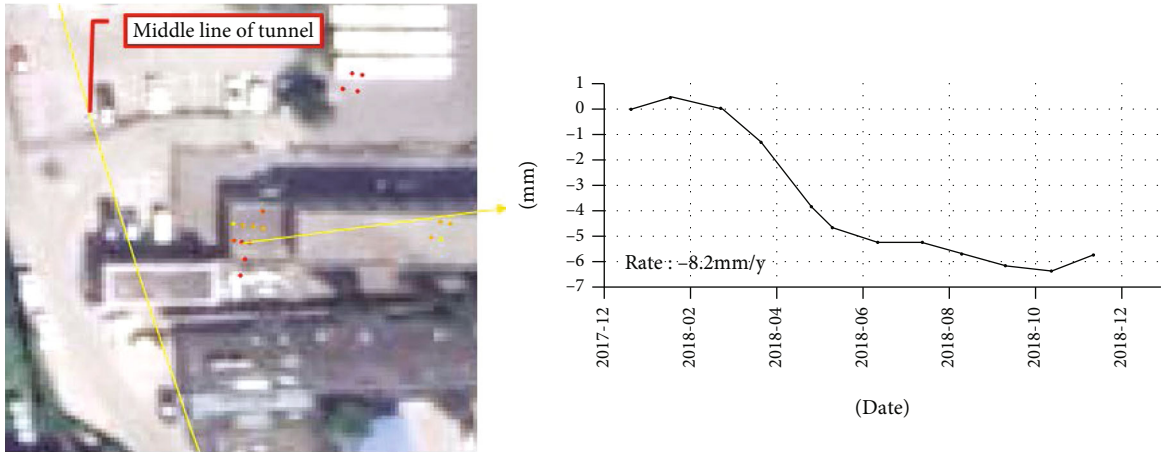

Figure 29: Position relation between building B and the middle line of the tunnel and the displacement time series of a PS point on the building.

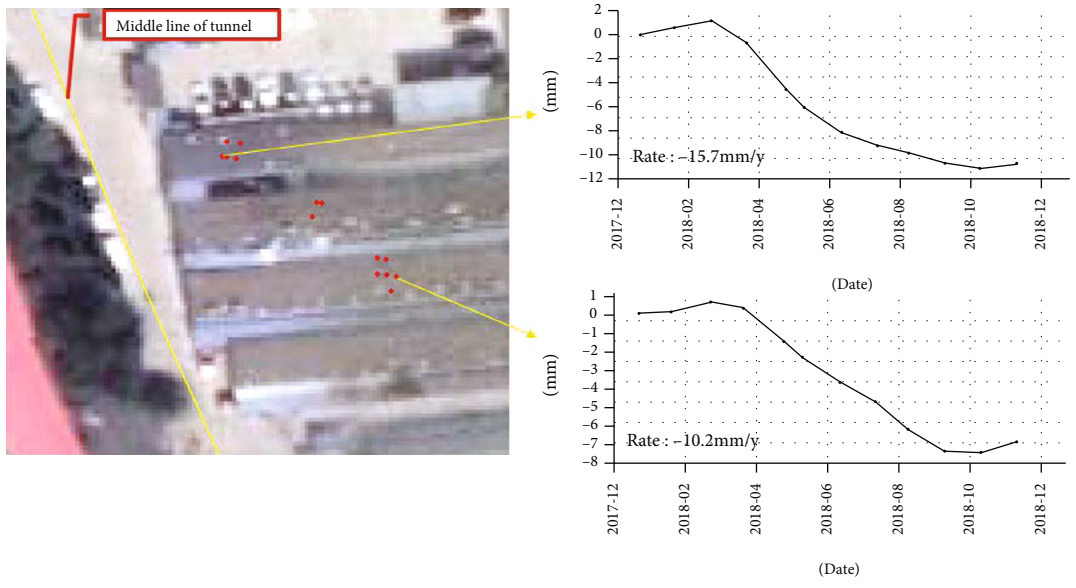

Figure 30: Position relation between building C and tunnel midline and the displacement time series at the PS point on the building.

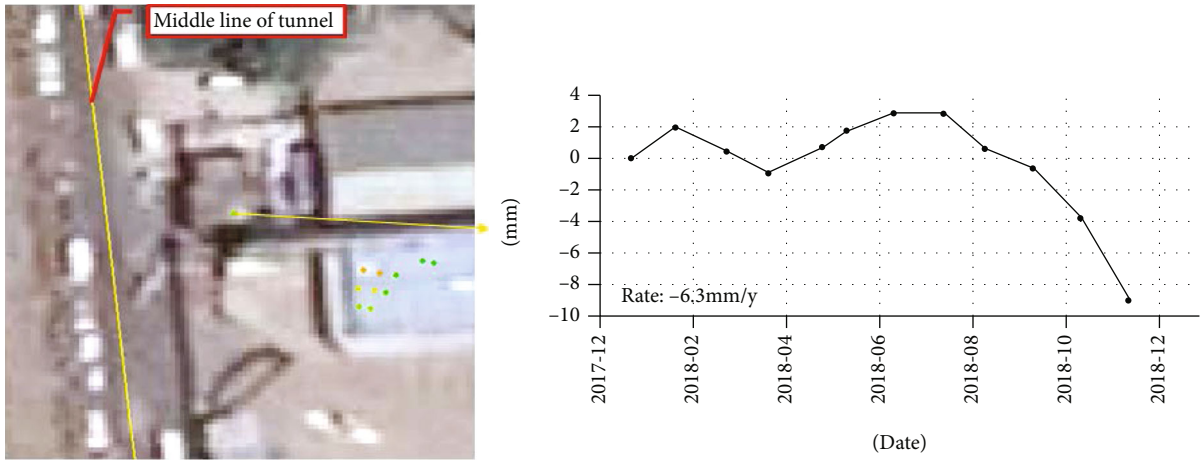

Figure 31: Position relation between building D and tunnel midline and the deformation time series of a PS point on the building.

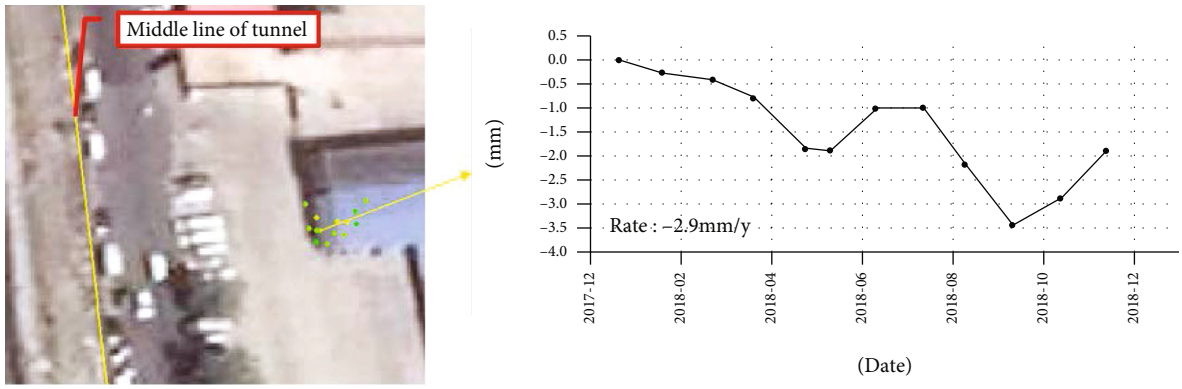

Figure 32: Position relation between building E and the middle line of tunnel and the deformation time-series of a PS point on the building.

6. Conclusions

In this paper, the subsidence characteristics of the surface and surrounding structures of shield tunnels are studied using the leveling measurements and InSAR measurements from CSK and Sentinel-1 data. A combined monitoring model of the overlying ground deformation of a shield tunnel is proposed. A number of important parameters for shield tunnel excavation, including the influence angle and distance in both longitudinal and transverse direction, the lag angle and distance of maximum subsidence rate, and their relationships with the width-depth ratio of shield tunnels during the excavation and the shield excavation subsidence time can be derived from the measurement results.

The deformation information of buildings around the shield tunnels and the influence characteristics of shield tunnels on buildings are investigated. Through the above analysis, the influence of shield tunneling excavation on the ground surface and surrounding infrastructure for the Beijing-Zhangjiakou high-speed railway is analyzed. The ground surface deformation characteristics of shield tunnel excavation can provide technical support and reference for future shield tunnel excavation works; this is important for ensuring the safety of people's lives and property around shield tunnels.

Data Availability

The COSMO-SkyMed data used to support the findings of this study have not been made available because they are commercial satellite data. The ESA for providing the Sentinel-1 data are available because they are open data, which can be downloaded from the ESA official website. The field surveying data used to support the findings of this study have not been made available because they are confidential data according Chinese law.

Conflicts of Interest

The authors declare no conflict of interest.

Authors' Contributions

Yueguan Yan and Qian Yang designed the experiments and analyzed the InSAR data and wrote the manuscript, Xiaoyi Zhang provided and analyzed the field data, and Huayang Dai and Alex Hay-Man Ng revised and edited the manuscript. All authors provided critical feedback and helped shape the research, analysis, and manuscript.

Acknowledgments

The authors thank ASI for providing the COSMO-SkyMed data and ESA for providing the Sentinel-1 data. The authors would also like to thank the Beijing Tianjin Project Management Ltd. for providing the field surveying data and the geospatial data and the permission to include them in this manuscript. This research was funded by the National Natural Science Foundation of China (grant numbers 51574242 and 51404272), Natural Science Foundation of Guangdong Province (grant numbers 2018A030310538 and 2021A1515011483), Science and Technology Program of Guangzhou (grant number 201904010254), and Program for Guangdong Introducing Innovative and Entrepreneurial Teams (2019ZT08L213). This research is also supported by the Fundamental Research Funds for the Central Universities (2021YQDC09).

References

[1] Y. Bao, Q. Zheng, J. Tang et al., "Metro shield tunnel construction monitoring technology," *Railway Architecture*, vol. 5, pp. 44–47, 2009.

[2] S. Suwansawat and H. Herbert, "Artificial neural networks for predicting the maximum surface settlement caused by EPB shield tunneling," *Tunnelling and Underground Space Technology*, vol. 21, no. 2, pp. 133–150, 2006.

[3] S. Suwansawat and H. H. Einstein, "Describing settlement troughs over twin tunnels using a superposition technique," *Journal of Geotechnical and Geoenvironmental Engineering*, vol. 133, no. 4, pp. 445–468, 2007.

[4] L. Tao, C. Guan, Y. Zhang, and W. Li, "Prediction of surface subsidence in shield tunnel excavation by improved GAP method," *Journal of Liaoning Technical University*, pp. 166–169, 2013.

[5] W. Li, "Analysis and regularity of ground subsidence caused by shield tunneling in metro tunnels," *Journal of Vibroengineering*, vol. 22, pp. 1126–1144, 2015.

[6] H. Fattahi and N. Babanouri, "RES-based model in evaluation of surface settlement caused by EPB shield tunneling," *Indian Geotechnical Journal*, vol. 48, no. 4, pp. 746–752, 2018.

[7] A. H.-M. Ng, H. Wang, Y. Dai et al., "InSAR reveals land deformation at Guangzhou and Foshan, China between 2011 and 2017 with COSMO-SkyMed data," *Remote Sensing*, vol. 10, no. 6, p. 813, 2018.

[8] A. Ferretti, C. Prati, and F. Rocca, "Permanent scatterers in SAR interferometry," *IEEE Transactions on Geoscience and Remote Sensing*, vol. 39, no. 1, pp. 8–20, 2001.

[9] Y. Zhang, G. Tang, and D. Lu, "Study on land subsidence monitoring of Beijing-Tianjin intercity railway based on PS-InSAR," *Surveying and Mapping and Spatial Geographic Information*, vol. 36, pp. 229–232, 2013.

[10] H.-B. Zhang, J.-J. Chen, F. Fan, and J.-H. Wang, "Deformation monitoring and performance analysis on the shield tunnel influenced by adjacent deep excavations," *Journal of Aerospace Engineering*, vol. 30, article B4015002, 2015.

[11] H. Liu, Y. Zhang, R. Wang et al., "Land subsidence monitoring and result analysis of Beijing section of Beijing-Tianjin high-speed railway," *Journal of Geo-Information Science*, pp. 2424–2432, 2016.

[12] Y. Zhou, M. Chen, H. Gong, X. Li, J. Yu, and X. Zhu, "Land subsidence monitoring of Beijinssg section of Beijing-Tianjin high-speed railway based on time series InSAR," *Journal of Geo-Information Science*, pp. 137–147, 2017.

[13] Y. Tang and K. Yang, "Application of InSAR technology in subsidence monitoring of shield tunnel section of Tianjin Metro Line 6," *Urban Survey*, pp. 109–113, 2018.

[14] Y. Chen, H. Dai, and Y. Yan, "Surface subsidence law of shallow-buried and subsurface excavation method in section of Beijing Metro Line 6," in *National Academic Conference on Mining under buildings, railways and waterbodies*, Chengdu, Sichuan, China, 2012.

[15] A. H.-M. Ng, L. Ge, and X. Li, "Assessments of land subsidence in the Gippsland Basin of Australia using ALOS PALSAR data," *Remote Sensing of Environment*, vol. 159, pp. 86–101, 2015.

[16] L. Ge, A. H.-M. Ng, X. Li, Z. Abidin, and I. Gumilar, "Land subsidence characteristics of Bandung Basin as revealed by ENVISAT ASAR and ALOS PALSAR interferometry," *Remote Sensing of Environment*, vol. 154, pp. 46–60, 2014.

[17] P. Ma and H. Lin, "Robust detection of single and double persistent scatterers in urban built environments," *IEEE Transactions on Geoscience and Remote Sensing*, vol. 54, no. 4, pp. 2124–2139, 2016.

[18] K. Yanagiya and M. Furuya, "Post-wildfire surface deformation near Batagay, Eastern Siberia, detected by L-band and C-band InSAR," *Journal of Geophysical Research: Earth Surface*, vol. 125, no. 7, article e2019JF005473, 2020.

[19] K. J. Reinders, R. F. Hanssen, F. J. van Leijen, and M. Korff, "Augmented satellite InSAR for assessing short-term and long-term surface deformation due to shield tunnelling," *Tunnelling and Underground Space Technology*, vol. 110, article 103745, 2021.

[20] S. L. Furst, S. Doucet, P. Vernant, C. Champollion, and J. L. Carme, "Monitoring surface deformation of deep salt mining in Vauvert (France), combining InSAR and leveling data for multi-source inversion," *Solid Earth*, vol. 12, no. 1, pp. 15–34, 2021.

[21] W. Guo, W. Shan, C. Zhang, Z. Hu, S. Wang, and J. Gao, "Monitoring of permafrost degradation along the Bei'an-Heihe Expressway in China," *Bulletin of Engineering Geology and the Environment*, vol. 80, no. 1, pp. 1–10, 2021.

[22] D. C. Elizabeth, B. Andreas, and H. Volker, "Surface subsidence in urbanized coastal areas: PSI methods based on Sentinel-1 for Ho Chi Minh City," *Remote Sensing*, vol. 12, no. 24, article 4130, 2020.

[23] X. Zhang, J. Zhao, L. Xin, K. Wang, and H. Pan, "Monitoring and assessment of cemented paste backfill containing coal gangue and fly ash in an underground mine," *Advances in Materials Science and Engineering*, vol. 2021, 15 pages, 2021.

[24] China Ministry of Construction, *Code for Engineering Surveying (GB50026-2007)*, China Planning Press, 2008.

[25] A. H.-M. Ng, L. Ge, X. Li, and K. Zhang, "Monitoring ground deformation in Beijing, China with persistent scatterer SAR interferometry," *Journal of Geodesy*, vol. 86, no. 6, pp. 375–392, 2012.

[26] Q. Lin, J. Vesecky, and H. A. Zebker, "New approaches in interferometric SAR data processing," *IEEE Transactions on Geoscience and Remote Sensing*, vol. 30, no. 3, pp. 560–567, 1992.

[27] A. Ferretti, C. Prati, and F. L. Rocca, "Analysis of permanent scatterers in SAR interferometry," in *IEEE International Geoscience and Remote Sensing Symposium*, Honolulu, America, July 2000.